Available online at www.sciencedirect.com
ScienceDirect
Journal of Sound and Vibration 314 (2008) 275–306
JOURNAL OF SOUND AND VIBRATION
www.elsevier.com/locate/jsvi

Sound synthesis of a nonlinear string using Volterra series

Thomas Hélie[a,*], David Roze[a,b]

[a]*Analysis-Synthesis team, IRCAM-CNRS UMR 9912, 1 place Igor Stravinsky, 75004 Paris, France*
[b]*CEA-LIST, Route du panorama, 92265 Fontenay-aux-roses Cedex, France*

Received 20 August 2007; received in revised form 7 January 2008; accepted 7 January 2008
Handling Editor: M.P. Cartmell
Available online 7 March 2008

Abstract

This paper proposes to solve and simulate various Kirchhoff models of nonlinear strings using Volterra series. Two nonlinearities are studied: the string tension is supposed to depend either on the global elongation of the string (first model), or on the local strain located at x (second, and more precise, model). The boundary conditions are simple Dirichlet homogeneous ones or general dynamic conditions (allowing the string to be connected to any system; typically a bridge). For each model, a Volterra series is used to represent the displacement as a functional of excitation forces. The Volterra kernels are solved using a modal decomposition: the first kernel of the series yields the standard modes of the linearized problem while the next kernels introduce the nonlinear dynamics. As a last step, systematic identification of the kernels lead to a structure composed of linear filters, sums, and products which are well-suited to the sound synthesis, using standard signal processing techniques. The nonlinear dynamic introduced through this simulation is significant and perceptible in sound results for sufficiently large excitations.

1. Introduction

In musical acoustics, sound synthesis aims to produce a more and more realistic result for complex systems such as musical instruments. Usually, these instruments involve nonlinear propagation phenomena as soon as vibrations are sufficiently large in instruments such as gongs, dynamics of bowed strings, piano soundboards, etc. Thus, physical models which include nonlinear phenomena have been derived and usually solved using numerical methods, as in Ref. [1]. For sinusoidal type excitations, methods such as nonlinear modes [2,3] or the harmonic balance [4,5] are interesting alternatives.

In this article, nonlinear models of damped strings are solved using Volterra series (see Ref. [6,7]). This method allows both analytic and numerical solutions to be performed without requiring sinusoidal-type excitations. More precisely, once the analytic kernels of the series are derived, straightforward identifications lead to structures composed of linear filters, sums, and products. This yields efficient simulations from standard signal processing techniques, which are well-adapted to real-time synthesis. Moreover, decomposing the kernels on the modal basis yields original but natural interpretations: it exhibits precisely the nonlinear dynamics of each spatial mode.

*Corresponding author.
E-mail addresses: thomas.helie@ircam.fr (T. Hélie), david.roze@ircam.fr (D. Roze).

0022-460X/$ - see front matter © 2008 Published by Elsevier Ltd.
doi:10.1016/j.jsv.2008.01.038

Physical models of strings are numerous. Historically, the first information on the equations of the motion of a string appeared in the 18th century with the works of d'Alembert [8] and Euler [9] who, respectively, wrote the two linear partial differential equations for small vibrations of a string and transverse vibrations of a bar (see also Ref. [10]). During the 19th century, Kirchhoff derived a model of a one-dimensional perfectly flexible string, including a nonlinearity due to the variation of tension [11]. This model has been re-investigated by Carrier in Ref. [12] from which new string models of musical instruments have been elaborated. For instance, in Ref. [13], Anand focused on the non-planar transverse vibrations (with celerity c_l) and neglected the longitudinal ones (with celerity c_l), assuming that $c_l^2 \gg c_t^2$. On the other hand, in Ref. [14], Narasimha states that the longitudinal motion cannot be neglected even for small amplitudes. Both these works (and others) have been unified by Watzky in Ref. [15] with a three-dimensional model of a nonlinear stiff string. This generalization includes a torsion coupling and allows the introduction of inharmonicity using the hypothesis of a linear elastic behaviour. Advanced models and experimental results on strings can also be found in Ref. [16].

This work focuses on three mono-dimensional nonlinear models (M1,M2,M3) of perfectly flexible strings with large transverse waves: the nonlinearity can be globally integrated (M1,M2) or locally distributed (M3) in space; the boundary conditions can be homogeneous (M1,M3) or it is possible to connect the string to another system, typically, a bridge (M2).

The paper is organized as follows: Section 2 presents the three models; Section 3 introduces the Volterra series; Sections 4–6, detail the calculation of the Volterra kernels for (M1)–(M3), from which simulable structures are deduced. Section 7 presents results and comparisons in both the time and time–frequency domains. Section 8 develops conclusions and perspectives.

2. Physical models of strings

2.1. Geometry, physical constants, and excitation

Consider the displacement $u(x,t)$ of a perfectly flexible string (Fig. 1) with a length L (m), an initial tension T_0 (N), and a small circular section with radius R (m). The material is characterized by a density ρ ($\mathrm{kg\,m^{-3}}$), a Young's modulus E (Pa), a standard fluid damping δ ($\mathrm{s^{-1}}$) introduced by the transverse mass force $-\delta(\partial u/\partial t)$, and a structural damping κ ($\mathrm{m^2\,s^{-1}}$) introduced by $+\kappa(\partial^3 u/\partial t\partial x^2)$. These dampings model thermoelastic losses and viscoelasticity [17].

The string is supposed to be motionless before $t=0$ and the transverse displacement is denoted $u(x,t)$ for all $(x,t) \in \overline{\Omega} \times \mathbb{R}^+$ with $\Omega =]0,L[$ and $\overline{\Omega} = [0,L]$. It is excited by a transverse mass force $f_\phi(x,t) = \phi(x)f(t)$ where ϕ is positive and spatially distributes the total force $f(t)$, so that

$$\rho A \int_\Omega \phi(x)\,\mathrm{d}x = 1 \quad \text{with } A = \pi R^2. \tag{1}$$

Two simplified models of the nonlinear propagation (NL1,NL2) and two kinds of boundary conditions (B1,B2) are described below for transverse vibrations.

2.2. Nonlinear models of propagation, boundary and initial conditions

2.2.1. Model with a global variation of tension (NL1)

The Kirchhoff equation models the transverse vibrations of a string [11]. If the fluid and structural damping forces are included, it is given by

$$\forall (x,t) \in \Omega \times \mathbb{R}_+^\star, \quad \frac{\partial^2 u}{\partial t^2} + \delta\frac{\partial u}{\partial t} - \kappa\frac{\partial^3 u}{\partial t\partial x^2} = \left[c^2 + b\int_0^L \left(\frac{\partial u}{\partial x}\right)^2 \mathrm{d}x\right]\frac{\partial^2 u}{\partial x^2} + f_\phi, \tag{2}$$

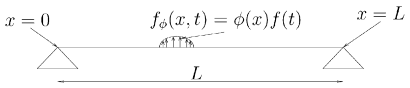

Fig. 1. Characteristics of the string.

where $c=\sqrt{T_0/\rho A}$ is the wave celerity ($\mathrm{m\,s^{-1}}$) and $b=E/2\rho L$ is the coefficient of the nonlinearity ($\mathrm{m\,s^{-2}}$) which takes into account the variation of tension. This model holds under three hypotheses [18]: (H1) the transverse vibrations are confined to a plane; (H2) the string is perfectly flexible (second-order equation); (H3) the nonlinear effects are due to the global variation of length.

2.2.2. Model with a local variation of tension (NL2)

The Kirchhoff–Carrier equations model both the longitudinal (v) and the transverse (u) vibrations which are coupled through the variation of tension. For an undamped string [12], they are given by, $\forall(x,t)\in\Omega\times\mathbb{R}_+^\star$,

$$\rho A\frac{\partial^2 u}{\partial t^2}=\frac{\partial}{\partial x}\left[\frac{T(\partial u/\partial x)}{\sqrt{(\partial u/\partial x)^2+(1+(\partial v/\partial x))^2}}\right]\quad\text{and}\quad\rho A\frac{\partial^2 v}{\partial t^2}=\frac{\partial}{\partial x}\left[\frac{T(1+(\partial v/\partial x))}{\sqrt{(\partial u/\partial x)^2+(1+(\partial v/\partial x))^2}}\right],\tag{3}$$

where $T-T_0=EA(\sqrt{(\partial u/\partial x)^2+(1+(\partial v/\partial x))^2}-1)$. Neglecting $\partial v/\partial x$ in Eq. (3a) and including the fluid and structural damping forces define the model (NL2) which governs a damped wave u decoupled from v:

$$\rho A\frac{\partial^2 u}{\partial t^2}+\rho A\delta\frac{\partial u}{\partial t}-\rho A\kappa\frac{\partial^3 u}{\partial t\partial x^2}=\frac{\partial}{\partial x}\left[\frac{(T_0+EA(\sqrt{1+(\partial u/\partial x)^2}-1))\partial u/\partial x}{\sqrt{1+(\partial u/\partial x)^2}}\right].\tag{4}$$

Note that this model involves a nonlinearity (local with respect to x) with no integral operator as in (NL1). In this model, (H3) is relaxed, but only transverse waves are (still) assumed to be significant.

This model (NL2) will illustrate how the solutions and the simulations are modified because of local—rather than global—nonlinearities. A more realistic model with coupled waves will be solved in a future work.

2.2.3. Boundary conditions (B1,B2) and initial conditions

Boundary conditions (B1) are homogeneous Dirichlet conditions, i.e. the string has no displacement at extremities:

$$\forall(x,t)\in\{0;L\}\times\mathbb{R}^+,\quad u(x,t)=0.\tag{5}$$

Boundary conditions (B2) are defined by

$$\forall(x,t)\in\{0;L\}\times\mathbb{R}^+,\quad u(x,t)=u_x(t),\tag{6}$$

where u_0 and u_L represent excitations. These excitations are both displacements but could be both forces ($\partial u/\partial x(x,t)=u_x(t)$ for $(x,t)\in\{0;L\}\times\mathbb{R}^+$), or even mixed excitations. These choices do not affect the method proposed in the following, but only the solutions. The latter conditions (B2) allow the string to be connected to a bridge or to other mechanical systems, at its extremities.

For all the cases studied here, the string is supposed to be motionless for $t\leqslant 0$ so that initial conditions are zero:

$$\forall(x,t)\in\Omega\times\{0\},\quad k\in\{0;1\},\quad\frac{\partial^k u}{\partial t^k}(x,t)=0.\tag{7}$$

2.3. Dimensionless models

The changes of variables and functions given in Table 1 yield the dimensionless models (M1,M2,M3) on $\widetilde{\Omega}=]0,1[$:

$(M1)\equiv(NL1,B1)$: Clamped string with a global variation of tension:

$$\forall(\tilde{x},\tilde{t})\in\tilde{\Omega}\times\mathbb{R}_+^\star,\quad\frac{\partial^2\tilde{u}}{\partial\tilde{t}^2}+\alpha\frac{\partial\tilde{u}}{\partial\tilde{t}}-\beta\frac{\partial^3\tilde{u}}{\partial\tilde{t}\partial\tilde{x}^2}=\left[1+\varepsilon\int_0^1\left(\frac{\partial\tilde{u}}{\partial\tilde{x}}\right)^2\mathrm{d}\tilde{x}\right]\frac{\partial^2\tilde{u}}{\partial\tilde{x}^2}+\tilde{f}_{\tilde{\phi}},\tag{8}$$

$$\forall(\tilde{x},\tilde{t})\in\{0;1\}\times\mathbb{R}_+^\star,\quad\tilde{u}(\tilde{x},\tilde{t})=0,\tag{9}$$

Table 1
Changes of variables, of functions, and of dimensionless coefficients (Eq. (1) translates into $\int_0^1 \tilde{\phi}(\tilde{x})\,\mathrm{d}\tilde{x} = 1$)

Dimensional		Dimensionless	
Geometry	Physical constants	Variables/coefficients	Functions
$L = 1.8\,\mathrm{m}$	$\rho = 7800\,\mathrm{kg\,m^{-3}}$	$\tilde{x} = \frac{x}{L},\ \tilde{t} = \frac{tc}{L}$	$\tilde{u}(\tilde{x},\tilde{t}) = \frac{u(\tilde{x}L, \frac{\tilde{t}L}{c})}{U^\star}$
$R = 1.5\,\mathrm{mm}$	$E = 2\times10^{11}\,\mathrm{Pa}$	$\alpha = \frac{\delta L}{c} = 5.45\times10^{-2}$	$\tilde{\phi}(\tilde{x}) = \rho\pi R^2 L\phi(\tilde{x}L)$
Reference	$\delta = 3\,\mathrm{s^{-1}}$	$\beta = \frac{\kappa}{cL} = 2.81\times10^{-5}$	$\tilde{f}(\tilde{t}) = \frac{Lf\left(\frac{\tilde{t}L}{c}\right)}{\rho\pi R^2 c^2 U^\star}$
displacement:	$\kappa = 0.01\,\mathrm{m^2\,s^{-1}}$	$\varepsilon = \frac{E(U^\star)^2}{2\rho(Lc)^2} = 2.27\times10^{-4}$	$\tilde{f}_{\tilde{\phi}}(\tilde{x},\tilde{t}) = \tilde{\phi}(\tilde{x})\tilde{f}(\tilde{t})$
$U^\star = R$	$T_0 = 2161\,\mathrm{N}$	$\eta = \left(\frac{U^\star}{L}\right)^2 = 6.94\times10^{-7}$	$\tilde{u}_{\tilde{x}}(\tilde{t}) = \frac{u_{\tilde{x}L}(\frac{\tilde{t}L}{c})}{U^\star}$

The proposed values are used in Section 7: the string is made of steel [19,20]; δ, κ, and T_0 are tuned to have realistic damped sounds and the fundamental frequency $f = c/2L = 55\,\mathrm{Hz}$ with $c = \sqrt{T_0/\rho A}$.

$$\forall(\tilde{x},\tilde{t}) \in \tilde{\Omega}\times\{0\},\quad \tilde{u}(\tilde{x},\tilde{t}) = 0 \quad\text{and}\quad \frac{\partial\tilde{u}}{\partial\tilde{t}}(\tilde{x},\tilde{t}) = 0. \tag{10}$$

$(M2) \equiv (NL1, B2)$: Same string with dynamic boundary conditions:

$$\forall(\tilde{x},\tilde{t}) \in \tilde{\Omega}\times\mathbb{R}_+^\star,\quad \frac{\partial^2\tilde{u}}{\partial\tilde{t}^2} + \alpha\frac{\partial\tilde{u}}{\partial\tilde{t}} - \beta\frac{\partial^3\tilde{u}}{\partial\tilde{t}\partial\tilde{x}^2} = \left[1 + \varepsilon\int_0^1\left(\frac{\partial\tilde{u}}{\partial\tilde{x}}\right)^2\mathrm{d}\tilde{x}\right]\frac{\partial^2\tilde{u}}{\partial\tilde{x}^2} + \tilde{f}_{\tilde{\phi}}, \tag{11}$$

$$\forall(\tilde{x},\tilde{t}) \in \{0;1\}\times\mathbb{R}_+^\star,\quad \tilde{u}(\tilde{x},\tilde{t}) = \tilde{u}_{\tilde{x}}(\tilde{t}), \tag{12}$$

$$\forall(\tilde{x},\tilde{t}) \in \tilde{\Omega}\times\{0\},\quad \tilde{u}(\tilde{x},\tilde{t}) = 0 \quad\text{and}\quad \frac{\partial\tilde{u}}{\partial\tilde{t}}(\tilde{x},\tilde{t}) = 0. \tag{13}$$

$(M3) \equiv (NL2, B1)$: Clamped string with local variations of tension:

$$\forall(\tilde{x},\tilde{t}) \in \tilde{\Omega}\times\mathbb{R}_+^\star,\quad \frac{\partial^2\tilde{u}}{\partial\tilde{t}^2} + \alpha\frac{\partial\tilde{u}}{\partial\tilde{t}} - \beta\frac{\partial^3\tilde{u}}{\partial\tilde{t}\partial\tilde{x}^2} = \frac{\partial}{\partial\tilde{x}}\left[\frac{(1-(2\varepsilon/\eta))(\partial\tilde{u}/\partial\tilde{x})}{\sqrt{1+\eta(\partial\tilde{u}/\partial\tilde{x})^2}} + \frac{2\varepsilon}{\eta}\frac{\partial\tilde{u}}{\partial\tilde{x}}\right] + \tilde{f}_{\tilde{\phi}}, \tag{14}$$

$$\forall(\tilde{x},\tilde{t}) \in \{0;1\}\times\mathbb{R}_+^\star,\quad \tilde{u}(\tilde{x},\tilde{t}) = 0, \tag{15}$$

$$\forall(\tilde{x},\tilde{t}) \in \tilde{\Omega}\times\{0\},\quad \tilde{u}(\tilde{x},\tilde{t}) = 0 \quad\text{and}\quad \frac{\partial\tilde{u}}{\partial\tilde{t}}(\tilde{x},\tilde{t}) = 0. \tag{16}$$

For sake of legibility, *the tilde symbols will be omitted in the following.*

3. Introduction to Volterra series

Volterra series have been mainly used to solve nonlinear electronic circuits and ordinary differential equations including regular nonlinearities (see Refs. [21–24]). They represent the solution (for "control engineers", the output of a system) as an infinite sum of multi-convolutions fed by the excitation (the input of a system). It extends "linear filtering" to the case of "weakly nonlinear behaviours".

3.1. Definition and properties

A causal system (in the "control engineers' meaning") with input f, output u (see Fig. 2) is described by a Volterra series with kernels $\{h_n\}_{n\in\mathbb{N}^*}$ if

$$\forall t\in\mathbb{R}^+,\quad u(t)=\sum_{n=1}^{\infty}\int_{(\mathbb{R}^+)^n} h_n(\tau_{1:n})f(t-\tau_1)\dots f(t-\tau_n)\,\mathrm{d}\tau_{1:n}, \tag{17}$$

with the notation $(\tau_{1:n})=(\tau_1,\tau_2,\dots,\tau_n)$ and $\mathrm{d}\tau_{1:n}=\mathrm{d}\tau_1\mathrm{d}\tau_2\cdots\mathrm{d}\tau_n$.

Eq. (17) can be interpreted as follows: for $n=1$, the term is a standard linear convolution so that h_1 is the impulse response of the linear contribution. For $n=2$, the term introduces a quadratic contribution of f on the output u. More generally, the nth term is associated with a homogeneous nonlinearity of order n which takes into account some memory through a "multi-convolution".

Moreover, as in the linear case, generalized transfer functions $H_n(s_{1:n})$ (denoted with capital letters) can be defined as the Laplace transform of the generalized impulse responses $h_n(\tau_{1:n})$ ($(s_{1:n})=(s_1,\dots,s_n)$ denotes the Laplace variables). For a damped (i.e. stable) causal system, they are defined by

$$\forall(s_{1:n})\in\mathscr{D}\supset(\mathbb{C}_0^+)^n,\quad H_n(s_{1:n})=\int_{(\mathbb{R}^+)^n} h_n(\tau_{1:n})\mathrm{e}^{-(s_1\tau_1+\cdots+s_n\tau_n)}\,\mathrm{d}\tau_{1:n},$$

where $\mathscr{D}$ is the domain of definition and $\mathbb{C}_0^+$ is the set of complex numbers with a strictly positive real part (see Refs. [25, (29.1.2); 22] for more details).

Remark 1. Embedded Volterra series are: (a) linear filters ($h_n=0$ for $n\geqslant 2$); (b) instantaneous functions $u(t)=h(f(t))$ which admits a series expansion $h(f)=\sum_{n=1}^{+\infty}\alpha_n f^n$; (c) their combinations (sum, product, cascade, see Section 3.2).

Remark 2. For the case (b), $h_n(\tau_{1:n})=\alpha_n\delta(\tau_{1:n})$ in the time domain (δ denotes the Dirac distribution), and $H_n(s_{1:n})=\alpha_n$ in the Laplace domain.

Remark 3. For inputs f which are zero before $t=0$, Eq. (17) becomes $u(t)=\sum_{n=1}^{\infty}\int_{[0,t]^n} h_n(\tau_{1:n})f(t-\tau_1)\dots f(t-\tau_n)\,\mathrm{d}\tau_{1:n}$. Such a dynamic is that of a system with null initial conditions. This limitation can be removed using a more general definition of Volterra series (see Ref. [24]).

Remark 4. From a mathematical point of view, the convergence of the series holds for inputs f such that $|f(t)|<\rho$ where ρ is the convergence radius of the characteristic function $\varphi_h(x)=\sum_{n=1}^{+\infty}\|h_n\|_1 x^n$ with the L^1-norm $\|h_n\|_1=\int_{\mathbb{R}^n}|h_n(\tau_{1:n})|\mathrm{d}\tau_{1:n}$ (see Ref. [22]). In this case, $|u(t)|\leqslant\phi_h(\sup_{t\in\mathbb{R}}|f(t)|)$ (see Refs. [24,26,27] for other results on the convergence). Nevertheless, *we will not study the convergence of the Volterra series in this paper*: in practice, low-order truncations of the series yield good approximations, if the nonlinearity is not activated by "too large inputs", as discussed in Section 7.

3.2. Interconnection laws

The following interconnection laws will be useful to solve (M1)–(M3).

Consider two Volterra series with kernels $\{a_n\}_{n\in\mathbb{N}^*}$ and $\{b_n\}_{n\in\mathbb{N}^*}$. The systems with input f and output u defined, respectively, in Figs. 3 and 4 and, if $b_n=0$ for $n\geqslant 2$, in Fig. 5 are still described by a Volterra series. Their kernels $\{c_n\}_{n\in\mathbb{N}^*}$ are given in the Laplace domain, respectively [22, pp. 34,35] by

$$C_n(s_{1:n})=A_n(s_{1:n})+B_n(s_{1:n}), \tag{18}$$

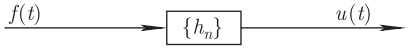

Fig. 2. System with input f and output u described by a Volterra series $\{h_n\}_{n\in\mathbb{N}^*}$.

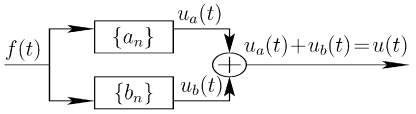

Fig. 3. Interconnection: sum of outputs.

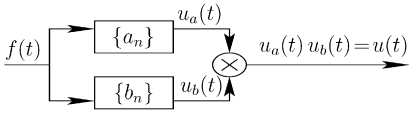

Fig. 4. Interconnection: product of outputs.

Fig. 5. Interconnection: cascade of a Volterra system with a linear system.

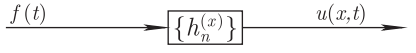

Fig. 6. Volterra system representing the solution $u(x,t)$ of (M1).

$$C_n(s_{1:n}) = \sum_{p=1}^{n-1} A_p(s_{1:p}) B_{n-p}(s_{p+1:n}), \tag{19}$$

$$C_n(s_{1:n}) = A_n(s_{1:n}) B_1(\widehat{s_{1:n}}), \tag{20}$$

with the notation $\widehat{s_{1:n}} = s_1 + \cdots + s_n$.

4. Solution and simulation of (M1) using a Volterra series

In this section, the displacement $u(x,t)$ of a string governed by (M1) and driven by a force f starting from $t = 0$ is solved. The spatial distribution ϕ is considered as an a priori given data of the problem. In Section 4.1, the Volterra series which maps f to u is defined. In Section 4.2, the kernels of the series are solved and explicit expressions are given. In Section 4.3, structures composed for linear filters, sums and products are identified from which a numerical simulation is derived.

4.1. Derivation of the Volterra kernels for (M1)

4.1.1. Modelling the solution by a Volterra series

Consider the displacement $u(x,t)$ as the output of a system (in the "control engineers' meaning") with input $f(t)$. This defines a nonlinear system that depends on the space variable x so that the corresponding Volterra series has kernels parameterized by x, denoted $h_n^{(x)}$ (see Fig. 6). The solution is represented by

$$\forall (x,t) \in \overline{\Omega} \times \mathbb{R}^+, \quad u(x,t) = \sum_{n=1}^{\infty} \int_{[0,t]^n} h_n^{(x)}(\tau_{1:n}) f(t-\tau_1) \ldots f(t-\tau_n)\, \mathrm{d}\tau_{1:n}. \tag{21}$$

Note that, from Remark 3 in Section 3.1, this solution naturally satisfies Eq. (10).

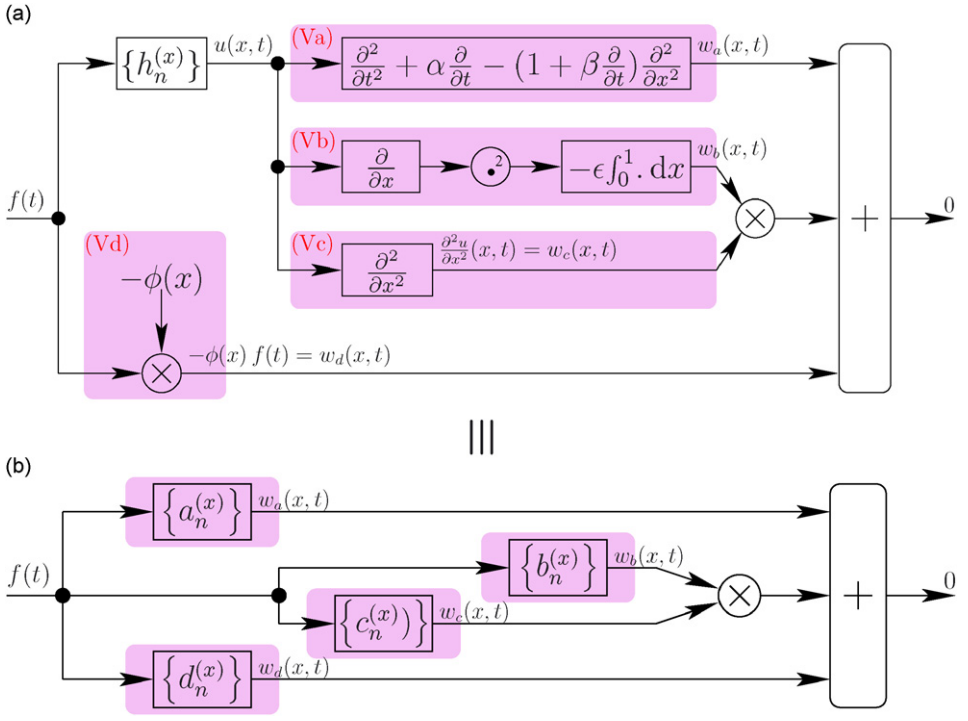

Fig. 7. Equivalent block-diagrams representing Eq. (8).

4.1.2. Equation satisfied by the kernels inside the domain Ω.

Eq. (8) requires that the kernels $h_n^{(x)}$ satisfy an equation inside Ω. This equation can be derived in the Laplace domain using the interconnection laws (see Section 3.2), as detailed below.

The block-diagram in Fig. 7(a) translates Eq. (8) into $w_a(x,t)+w_b(x,t)w_c(x,t)+w_d(x,t)=0$, where $w_a=(\partial^2u/\partial t^2)+\alpha(\partial u/\partial t)-(1+\beta(\partial/\partial t))(\partial^2u/\partial x^2)$, $w_b=-\varepsilon\int_0^1(\partial u/\partial x)^2\,\mathrm{d}x$, $w_c=\partial^2u/\partial x^2$, $w_d(x,t)=\phi(x)f(t)$, and where u is represented by Eq. (21).

Each system which maps f to $w_{\{a,b,c,d\}}$ can be represented by a Volterra series (see Fig. 7(b)), the kernels of which can be deduced from interconnection laws, in the Laplace domain, as follows:

Block (*Va*): in the Laplace domain (with respect to the time variable), the operator $(\partial^2/\partial t^2)+\alpha(\partial/\partial t)-(1+\beta(\partial/\partial t))(\partial^2/\partial x^2)$ becomes $s^2+\alpha s-(1+\beta s)\partial^2/\partial x^2$. Thus, from Eq. (20), the cascade of $\{H_n^{(x)}\}$ and this linear operator defines the Volterra series $\{A_n^{(x)}\}$ (see Fig. 7(b)) with, for all $n\in\mathbb{N}^*$,

$$A_n^{(x)}(s_{1:n})=\left[(\widehat{s_{1:n}})^2+\alpha\widehat{s_{1:n}}-(1+\beta\widehat{s_{1:n}})\frac{\partial^2}{\partial x^2}\right]H_n^{(x)}(s_{1:n}).$$

Note that, indeed, the spatial operator $\partial^2/\partial x^2$ can be applied on $h_n^{(x)}$ (and $H_n^{(x)}$) since it commutes with time operators (and their Laplace transform)[1]:

$$\begin{aligned}\frac{\partial^2u(x,t)}{\partial x^2}&=\frac{\partial^2}{\partial x^2}\sum_{n=1}^{\infty}\int_{[0,t]^n}h_n^{(x)}(\tau_{1:n})f(t-\tau_1)\dots f(t-\tau_n)\,\mathrm{d}\tau_{1:n}\\&=\sum_{n=1}^{\infty}\int_{[0,t]^n}\frac{\partial^2h_n^{(x)}(\tau_{1:n})}{\partial x^2}f(t-\tau_1)\dots f(t-\tau_n)\,\mathrm{d}\tau_{1:n}.\end{aligned}$$

[1]This holds under the standard hypotheses of the Lebesgue's dominated convergence theorem (see e.g. Ref. [28]) and the Leibniz integral rule (see e.g. Ref. [25, (3.3.7)]).

Block (*Vb*): Similarly, the cascade of $\{H_n^{(x)}(s_{1:n}\}$ and the linear spatial operator $\partial/\partial x$ defines the kernels $\partial H_n^{(x)}(s_{1:n})/\partial x$. Then, from Eq. (19), the cascade with the square yields $\sum_{p=1}^{n-1}(\partial/\partial x)H_p^{(x)}(s_{1:p})(\partial/\partial x)H_{n-p}^{(x)}(s_{p+1:n})$. Finally, the cascade with the spatial integral operator $-\varepsilon\int_\Omega \mathrm{d}x$ defines the Volterra series $\{B_n^{(x)}\}$ (see Fig. 7(b)) with, for all $n\in\mathbb{N}^*$,

$$B_n^{(x)}(s_{1:n}) = -\varepsilon\int_0^1 \sum_{p=1}^{n-1}\frac{\partial}{\partial x}H_p^{(x)}(s_{1:p})\frac{\partial}{\partial x}H_{n-p}^{(x)}(s_{p+1:n})\,\mathrm{d}x.$$

Block (*Vc*): The cascade of $H_n^{(x)}$ with $\partial^2/\partial x^2$ leads to the kernels

$$C_n^{(x)}(s_{1:n}) = \frac{\partial^2}{\partial x^2}H_n^{(x)}(s_{1:n}).$$

Block (*Vd*): For this case, $w_d(x,t) = -\phi(x)f(t) = \int_{-\infty}^{\infty} d_1^{(x)}(\tau_1)f(t-\tau_1)\,\mathrm{d}\tau_1$ with $d_1^{(x)}(\tau_1) = -\phi(x)\delta(\tau_1)$ where δ denotes the Dirac distribution (with Laplace transform 1). Hence, the corresponding Volterra kernels in the Laplace domain are given by

$$D_n^{(x)}(s_{1:n}) = -\delta_{1,n}\phi(x),$$

where $\delta_{1,n}$ denotes the Kronecker symbol ($\delta_{i,j}$ equals 1 if $i=j$ and equals 0 else).

Using Eqs. (18) and (19), the Volterra kernels of the whole system in Fig. 7(b) are given by, for all $n\in\mathbb{N}^*$, $A_n^{(x)}(s_{1:n}) + \sum_{k=1}^{n-1}B_k^{(x)}(s_{1:k})C_{n-k}^{(x)}(s_{k+1:n}) + D_n^{(x)}(s_{1:n})$. Now, this system maps f to 0 so that it defines the zero system for which all the Volterra kernels are zero. This leads to the equation satisfied by $H_n^{(x)}(s_{1:n})$ inside Ω, for all $n\in\mathbb{N}^*:\forall(x,s_{1:n})\in\Omega\times(\mathbb{C}_0^+)^n$,

$$[\Gamma(\widehat{s_{1:n}})]^2 H_n^{(x)}(s_{1:n}) - \frac{\partial^2 H_n^{(x)}(s_{1:n})}{\partial x^2} = \frac{E_n^{(x)}(s_{1:n})}{1+\beta\widehat{s_{1:n}}}, \tag{22}$$

with

$$E_1^{(x)}(s_1) = \phi(x), \tag{23}$$

$$E_n^{(x)}(s_{1:n}) = \varepsilon\sum_{\substack{p,q,r\geqslant 1\\ p+q+r=n}}\int_0^1\left[\frac{\partial H_p^{(x)}(s_{1:p})}{\partial x}\frac{\partial H_q^{(x)}(s_{p+1:p+q})}{\partial x}\right]\mathrm{d}x\frac{\partial^2 H_r^{(x)}(s_{p+q+1:n})}{\partial x^2} \quad \text{if } n\geqslant 2 \tag{24}$$

and

$$\forall s\in\mathbb{C}_0^+,\quad \Gamma(s) = \sqrt{\frac{s^2+\alpha s}{1+\beta s}}. \tag{25}$$

For each $n\in\mathbb{N}^*$, Eq. (22) is a linear second-order differential equation on $H_n^{(x)}$ with respect to x. Indeed, kernels $E_n^{(x)}$ only involve $H_{p,q,r}^{(x)}$ with $p,q,r\leqslant n-1$.

4.1.3. Equations satisfied by the kernels at the boundaries

The boundary conditions Eq. (9) impose a null displacement at $x\in\{0;1\}$. This means that kernels $h_n^{(x)}$ are zero at $x\in\{0;1\}$ (see Fig. 8).

In the Laplace domain, this yields, for all $n\in\mathbb{N}^*$:

$$\forall(x,s_{1:n})\in\{0;1\}\times(\mathbb{C}_0^+)^n,\quad H_n^{(x)}(s_{1:n}) = 0. \tag{26}$$

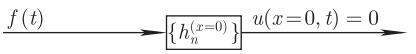

Fig. 8. Boundary condition on $h_n^{(x)}$ at $x=0$ (the same condition holds at $x=1$).

4.2. Solving the Volterra kernels

4.2.1. Analytic solution

For each $n\in\mathbb{N}^*$, Eqs. (22)–(26) define a linear boundary value problem, the solution of which is given by (see Appendix A.1),

$$\forall(x,s_{1:n})\in\Omega\times(\mathbb{C}_0^+)^n,\quad H_n^{(x)}(s_{1:n})=\int_\Omega G(x,\xi,\widehat{s_{1:n}})E_n^{(\xi)}(s_{1:n})\,\mathrm{d}\xi, \tag{27}$$

where, for all $(x,\xi,s)\in\Omega\times\Omega\times\mathbb{C}_0^+$,

$$G(x,\xi,s)=\frac{\cosh((1+x+\xi)\Gamma(s))-\cosh((1-|x-\xi|)\Gamma(s))}{2(1+\beta s)\Gamma(s)\sinh\Gamma(s)}. \tag{28}$$

Note that G does not depend on the choice of the square root for Γ since $\Gamma\mapsto-\Gamma$ keeps G invariant.

For $n=1$, this solution is exactly that of the linearized problem ((M1) with $\varepsilon=0$) where the Green function G is applied on the spatial distribution $E_1^{(x)}(s_1)=\phi(x)$ in the Laplace domain. For $n\geqslant 2$, $E_n^{(x)}$ involves kernels $H_p^{(x)}$ with $p\leqslant n-1$ (see Eq. (24)) so that Eq. (27) is a recurrence equation which makes the explicit derivation of analytic expressions possible. Nevertheless, in the following, we choose to use a modal decomposition: it helps to simplify these recurrent integral equations into recurrent algebraic equations.

4.2.2. Modal decomposition

For each $n\in\mathbb{N}^*$, the linear boundary value problem, Eqs. (22)–(26), admits an orthonormal basis of eigenfunctions $\mathscr{B}=\{e_k\}_{k\in\mathbb{N}^*}$ on the Hilbert space $L^2(\Omega)$ (see e.g. Ref. [29]). Functions e_k which define the spatial modes are

$$\forall(k,x)\in\mathbb{N}^*\times\Omega,\quad e_k(x)=\sqrt{2}\sin(k\pi x). \tag{29}$$

They satisfy: (i) the Dirichlet boundary conditions; (ii) $\partial^2 e_k/\partial x^2=-(k\pi)^2e_k$; (iii) for all $(i,j)\in(\mathbb{N}^*)^2$ $\langle e_i,e_j\rangle=\delta_{i,j}$ (Kronecker symbol) where the scalar product on $L^2(\Omega)$ is defined by $\forall(f,g)\in(L^2(\Omega))^2,\langle f,g\rangle=\int_\Omega f(x)g(x)\,\mathrm{d}x$.

Consider the decomposition of $H_n^{(x)}$ on $\mathscr{B}$, given by, for all $n\in\mathbb{N}^*$,

$$\forall(s_{1:n})\in(\mathbb{C}_0^+)^n,\quad H_n^{(x)}(s_{1:n})\underset{L^2}{=}\sum_{k\in\mathbb{N}^*}H_n^{[k]}(s_{1:n})e_k(x), \tag{30}$$

where $H_n^{[k]}=\langle H_n^{(x)},e_k\rangle$ denotes the projection of $H_n^{(x)}$ on e_k. The relations satisfied by $H_n^{[k]}$ are obtained by projecting Eqs. (22)–(24) on $\mathscr{B}$, as detailed in Appendix A.2. This yields the following algebraic equations, for all $(n,k)\in(\mathbb{N}^*)^2$, $(s_{1:n})\in(\mathbb{C}_0^+)^n$,

$$H_n^{[k]}(s_{1:n})=Q^{[k]}(\widehat{s_{1:n}})E_n^{[k]}(s_{1:n}), \tag{31}$$

$$E_1^{[k]}(s_1)=\langle\phi,e_k\rangle=\phi_k, \tag{32}$$

$$E_n^{[k]}(s_{1:n})=-\varepsilon k^2\pi^4\sum_{\substack{p,q,r\geqslant 1\\ p+q+r=n}}\left[\sum_{\ell\in\mathbb{N}^*}\ell^2H_p^{[\ell]}(s_{1:p})H_q^{[\ell]}(s_{p+1:p+q})\right]H_r^{[k]}(s_{p+q+1:n})\quad\text{if } n\geqslant 2, \tag{33}$$

where $Q^{[k]}(s)$ is the rational function given by

$$Q^{[k]}(s)=[s^2+(\alpha+\beta k^2\pi^2)s+k^2\pi^2]^{-1}, \tag{34}$$

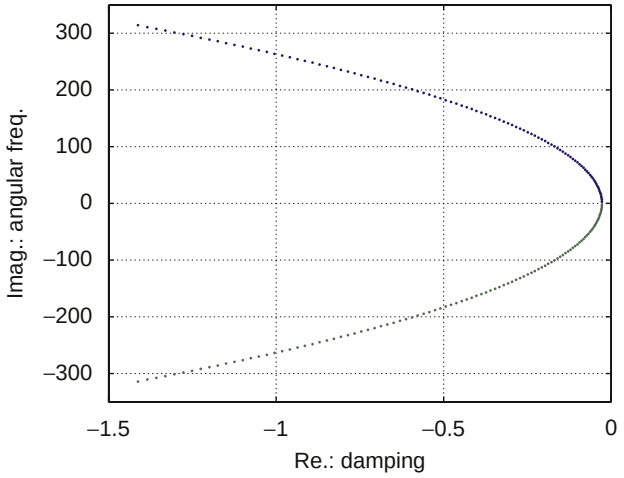

Fig. 9. Poles of $Q^{[k]}$ for $1 \leqslant k \leqslant K = 100$ and (α, β) given in Table 1.

which is analytic in $\mathbb{C}_0^+$. Indeed, for $\alpha \geqslant 0$ and $\beta \geqslant 0$, a straightforward analysis proves the real parts of the poles of $Q^{[k]}$ are all negative (or zero for the particular case $\alpha = \beta = 0$). More precisely, these poles correspond to damped oscillating modes if $1 \leqslant k < K^\star = 22,690$ (complex conjugated pair of poles) and purely evanescent ones if $k \geqslant K^\star$ (real negative poles). A detailed study of such an analysis can be found in Ref. [30] for the case of a bar with similar dampings. Fig. 9 represents the poles in the Laplace complex plane, for the typical values α and β given in Table 1.

Computing the analytic expressions for orders $n \in [1,5]_{\mathbb{N}}$ leads to, $\forall (k, s_{1:n}) \in \mathbb{N}^* \times (\mathbb{C}_0^+)^n$,

$$H_1^{[k]}(s_1) = \phi_k Q^{[k]}(s_1), \tag{35}$$

$$H_2^{[k]}(s_{1:2}) = 0, \tag{36}$$

$$H_3^{[k]}(s_{1:3}) = -\varepsilon k^2 \pi^4 Q^{[k]}(\widehat{s_{1:3}}) \left[\sum_{\ell \in \mathbb{N}^*} \ell^2 H_1^{(\ell)}(s_1) H_1^{(\ell)}(s_2) \right] H_1^{(k)}(s_3). \tag{37}$$

$$H_4^{[k]}(s_{1:4}) = 0, \tag{38}$$

$$\begin{aligned} H_5^{[k]}(s_{1:5}) = & -\varepsilon k^2 \pi^4 Q^{[k]}(\widehat{s_{1:5}}) \left[\sum_{\ell \in \mathbb{N}^*} \ell^2 H_3^{[\ell]}(s_{1:3}) H_1^{[\ell]}(s_4) H_1^{[k]}(s_5) \right. \\ & \left. + \sum_{\ell \in \mathbb{N}^*} \ell^2 H_1^{[\ell]}(s_1) H_3^{[\ell]}(s_{2:4}) H_1^{[k]}(s_5) + \sum_{\ell \in \mathbb{N}^*} \ell^2 H_1^{[\ell]}(s_1) H_1^{[\ell]}(s_2) H_3^{[k]}(s_{3:5}) \right]. \end{aligned} \tag{39}$$

Remark 5. For $n = 2$, the sum on $p, q, r \geqslant 1$ s.t. $p + q + r = n$ is empty so that, from Eq. (33), $E_n^{[k]}$ and $H_n^{(x)}$ are zero. More generally, a recurrence proves that for all $m \in \mathbb{N}^*$, $H_{2m}^{(x)} = 0$ and $H_{2m+1}^{(x)}$ is proportional to ε^m.

Remark 6. For $n = 1$, the solution leads to the standard modal decomposition of the linearized problem. For orders $n \geqslant 2$, Eqs. (31), (33) and (34) show how the dynamics of lower orders ($1 \leqslant p, q, r \leqslant n-1$ s.t. $p + q + r = n$) generate the nonlinear dynamics of order n. Eq. (33) also indicates what spatial modes contribute to the dynamics of order n of the mode k: all the modes $\ell \in \mathbb{N}^*$ contribute to the elongation (through the orders p and q) while the dynamics of order r (which contribute to the laplacian) are only those of the mode k.

4.2.3. Combinatorics, trees, and physical interpretations

The combinatorics due to Eqs. (30)–(33) can be reorganized as one summation of elementary terms, the indexes of summation being naturally described by full$^{(*)}$ ternary$^{(**)}$ trees,[2] as detailed below.

Definition 1. Let $\mathbb{A}_n$ be the sets of ternary trees defined by, for $n \in \mathbb{N}^*$,

$$\mathbb{A}_n = \mathbb{N}^* \quad \text{if } n = 1, \tag{40}$$

$$\mathbb{A}_n = \emptyset \quad \text{if } n \text{ is even}, \tag{41}$$

$$\mathbb{A}_n = \bigcup_{\substack{p,q,r\geqslant 1\\ p,q,r \text{ odd}\\ p+q+r=n}} \{(\mathfrak{a}_1,\mathfrak{a}_2,\mathfrak{a}_3) \in \mathbb{A}_p \times \mathbb{A}_q \times \mathbb{A}_r | \mathfrak{k}(\mathfrak{a}_1) = \mathfrak{k}(\mathfrak{a}_2)\} \quad \text{if } n \geqslant 3 \text{ is odd}, \tag{42}$$

where $\mathfrak{k}(\mathfrak{a})$ is the right-sided leaf of $\mathfrak{a}$: for $\mathfrak{a} = k \in \mathbb{A}_1$, $\mathfrak{k}(\mathfrak{a}) = k$; for $\mathfrak{a} = (\mathfrak{a}_1,\mathfrak{a}_2,\mathfrak{a}_3) \in \mathbb{A}_n$ (with $n \geqslant 3$), $\mathfrak{k}(\mathfrak{a}) = \mathfrak{k}(\mathfrak{a}_3)$. Moreover, $\mathfrak{n}(\mathfrak{a})$ denotes the number of leaves of $\mathfrak{a}$ so that if $\mathfrak{a} \in \mathbb{A}_n$ and if n is odd, $\mathfrak{n}(\mathfrak{a}) = n$.

Examples. $\overset{\mathfrak{a}}{\underset{8}{|}}$ denotes the tree $\mathfrak{a} \in \mathbb{A}_1$ such that $\mathfrak{k}(\mathfrak{a}) = 8$.

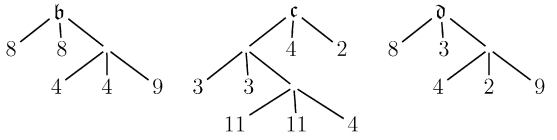

represent ternary trees $\mathfrak{b}$, $\mathfrak{c}$ and $\mathfrak{d}$ such that: $\mathfrak{k}(\mathfrak{b}) = 9$, $\mathfrak{n}(\mathfrak{b}) = 5$, $\mathfrak{b} \in \mathbb{A}_5$; $\mathfrak{k}(\mathfrak{c}) = 2$, $\mathfrak{n}(\mathfrak{c}) = 7$, $\mathfrak{c} \in \mathbb{A}_7$; $\mathfrak{k}(\mathfrak{d}) = 9$, $\mathfrak{n}(\mathfrak{d}) = 5$ but note that $\mathfrak{d} \notin \mathbb{A}_5$. Indeed, $\mathfrak{d} = (\mathfrak{d}_1,\mathfrak{d}_2,\mathfrak{d}_3)$ with $\mathfrak{d}_1 = 8$, $\mathfrak{d}_2 = 3$ and $\mathfrak{d}_3 = (4,2,9)$ so that, in Eq. (42), the condition $\mathfrak{k}(\mathfrak{a}_1) = \mathfrak{k}(\mathfrak{a}_2)$ is not satisfied (twice): first, because $\mathfrak{k}(\mathfrak{d}_1) = 8 \neq 3 = \mathfrak{k}(\mathfrak{d}_2)$; second, because $\mathfrak{d}_3 \notin \mathbb{A}_3$ for a similar reason ($4 \neq 2$).

Theorem 1. *For all $n \in \mathbb{N}^*$, kernels $H_n^{(x)}$ are given by, for all $(s_{1:n}) \in (\mathbb{C}_0^+)^n$,*

$$H_n^{(x)}(s_{1:n}) = \sum_{\mathfrak{a}\in\mathbb{A}_n} H_{\mathfrak{a}}(s_{1:n}) e_{\mathfrak{k}(\mathfrak{a})}(x), \tag{43}$$

where, for all $\mathfrak{a} \in \mathbb{A}_n$ (with n odd),

$$\text{if } n = 1, \quad H_{\mathfrak{a}}(s_1) = \phi_{\mathfrak{k}(\mathfrak{a})} Q^{[\mathfrak{k}(\mathfrak{a})]}(s_1), \tag{44}$$

$$\begin{aligned}\text{if } n \geqslant 3, \quad H_{\mathfrak{a}}(s_{1:n}) = &-\varepsilon[\mathfrak{k}(\mathfrak{a}_1)\mathfrak{k}(\mathfrak{a}_3)\pi^2]^2 Q^{[\mathfrak{k}(\mathfrak{a})]}(\widehat{s_{1:n}}) H_{\mathfrak{a}_1}(s_{1:\mathfrak{n}(\mathfrak{a}_1)})\\ &\times H_{\mathfrak{a}_2}(s_{\mathfrak{n}(\mathfrak{a}_1)+1:\mathfrak{n}(\mathfrak{a}_1)+\mathfrak{n}(\mathfrak{a}_2)}) H_{\mathfrak{a}_3}(s_{\mathfrak{n}(\mathfrak{a}_1)+\mathfrak{n}(\mathfrak{a}_2)+1:n}) \text{ with } \mathfrak{a} = (\mathfrak{a}_1,\mathfrak{a}_2,\mathfrak{a}_3).\end{aligned} \tag{45}$$

The proof of this theorem is detailed in Appendix A.3.

Interpretation: The trees memorize and isolate each elementary inheritance that each modal linear kernels transmit to a nth order kernel. For example, kernel $H_{\mathfrak{e}}$ with $\mathfrak{e} = (4,4,9) \in \mathbb{A}_n$ and $n = 3$ models how the elongation due to the linear dynamics of the mode 4 acts on the linear dynamics of mode 9 and contributes to its nonlinear dynamics of order $n = 3$. Kernel $H_{\mathfrak{b}}$ ($\mathfrak{b} = (8,8,\mathfrak{e}) \in \mathbb{A}_n$ with $n = 5$) models how that of mode 8 acts on the dynamics due to $H_{\mathfrak{e}}$ (order 3, mode 9) and contributes to the dynamics (mode 9) of order $n = 5$. More generally, for $\mathfrak{f} = (\mathfrak{f}_1,\mathfrak{f}_2,\mathfrak{f}_3) \in \mathbb{A}_n$ ($n \geqslant 3$, odd), $H_{\mathfrak{f}}$ models how the elongation introduced by the couple of dynamics due to $(H_{\mathfrak{f}_1}, H_{\mathfrak{f}_1})$ for the same mode $k = \mathfrak{k}(\mathfrak{f}_1) = \mathfrak{k}(\mathfrak{f}_2)$ acts on the dynamics due to $H_{\mathfrak{f}_3}$ (order $\mathfrak{n}(\mathfrak{f}_3)$, mode $\mathfrak{k}(\mathfrak{f}_3)$) and contributes to the dynamics of order n of the mode $\mathfrak{k}(\mathfrak{f}) = \mathfrak{k}(\mathfrak{f}_3)$.

Remark 7. Note that the condition $\mathfrak{k}(\mathfrak{a}_1) = \mathfrak{k}(\mathfrak{a}_2)$ in the definition Eq. (42) is due to the integral in Eq. (24) and the orthogonality of $\mathscr{B} = \{e_k\}_{k\in\mathbb{N}^*}$.

[2]This is linked to the nonlinearity of (M1) which is homogeneous$^{(*)}$ of degree $3^{(**)}$. Recall that a ternary tree is a tree in which every node has at most three children. A full ternary tree is a tree in which every node has zero or three children.

4.3. Identification of realizable structures for the sound synthesis

Computing the string dynamics from Eq. (21) using time-domain versions of Eqs. (43)–(45) leads to an infinite algorithmic complexity. In practice, infinite sums are truncated. First, only a finite number of modes are considered using $\widetilde{\mathbb{A}}_1 = [1, K]_{\mathbb{N}}$ in place of $\mathbb{A}_1$ in Definition 1. This yields good approximations in Eq. (43), if modes higher than K can be dropped due to negligible $\phi_k = \langle \phi, e_k \rangle$, or even, is exact if $\phi_k = 0$ for $k > K$. Second, only the first kernels $H_n^{(x)}$ for $1 \leqslant n \leqslant N = 2M + 1$ are kept in Eq. (21). This defines the approximation $\check{u}_N(x, t)$ such that $u(x, t) = \check{u}_N(x, t) + o(\varepsilon^M)$ (see Remark 5).

The realization theory allows to build structures which are well-adapted to the numerical simulation. For Volterra kernels, realizations can be performed from the regular Volterra kernels (see Ref. [23, Chapter 4] for a detailed presentation). Here, an alternative identification is proposed in Theorem 2, which does not require to compute the regular kernels. Then, realizations are deduced and detailed for orders $n = 1, 3, 5$.

4.3.1. Elementary ternary Volterra systems and identification theorem

Definition 2 (*Homogeneous Volterra system*). A Volterra system $\mathscr{S}$ with kernels $\{h_{n'}\}_{n' \in \mathbb{N}^*}$ is said to be "homogeneous" of order $n \in \mathbb{N}^*$, if h_n is non-zero, and if, for all $n' \in \mathbb{N}^* \backslash \{n\}$, the kernels $h_{n'}$ are null.

Note that linear filters are homogeneous systems of order 1.

Definition 3 (*Elementary ternary Volterra system*). A system $\mathscr{S}$ with input f and output u is an "elementary ternary Volterra system" if

- it exists three homogeneous Volterra systems $\mathscr{S}_a$, $\mathscr{S}_b$, $\mathscr{S}_c$, of respective order p, q, r, with respective output y_a, y_b, y_c, and all fed by the same input f,
- it exists a linear system $\mathscr{S}_d$,

such that u is the output of $\mathscr{S}_d$ fed by the input $w(t) = y_a(t)y_b(t)y_c(t)$ (see Fig. 10).

From interconnection laws Eqs. (19) and (20), the system $\mathscr{S}$ is proven to be homogeneous of order $n = p + q + r$: its kernel of order n is given by

$$H_n(s_{1:n}) = A_p(s_{1:p})B_q(s_{p+1:p+q})C_r(s_{p+q+1:n})D_1(\widehat{s_{1:n}}), \tag{46}$$

in the Laplace domain, where a_p, b_q, c_r, and d_1 denote the non-zero kernels of systems $\mathscr{S}_a$, $\mathscr{S}_b$, $\mathscr{S}_c$, and $\mathscr{S}_d$, respectively.

Theorem 2 (*Structure composed of filters, sums, and products*). *The solution* $u(x, t)$ *of* $(M1)$ *obtained from* Eqs. (21) *and* (43) *to* (45) *is given by the sum*

$$u(x, t) = \sum_{n \in \mathbb{N}^*} \sum_{\mathfrak{a} \in \mathbb{A}_n} u_{\mathfrak{a}}(t) e_{\mathfrak{f}(\mathfrak{a})}(x), \tag{47}$$

where the sub-dynamics signals $u_{\mathfrak{a}}$ *can be realized using linear filters and products, as follows*:

- *if* $\mathfrak{a} \in \mathbb{A}_1$, *then* $u_{\mathfrak{a}}$ *is the output of the linear filter with transfer function* $H_{\mathfrak{a}}(s)$ *given by Eq.* (44);
- *if* $n \geqslant 3$ *is odd and if* $\mathfrak{a} = (\mathfrak{a}_1, \mathfrak{a}_2, \mathfrak{a}_3) \in \mathbb{A}_n$, *then* $u_{\mathfrak{a}}$ *is the output of the linear filter with transfer function*

$$G_{\mathfrak{a}}(s) = -\varepsilon[\mathfrak{f}(\mathfrak{a}_1)\mathfrak{f}(\mathfrak{a}_3)\pi^2]^2 Q^{[\mathfrak{f}(\mathfrak{a})]}(s) \tag{48}$$

fed by the input $v_{\mathfrak{a}}(t) = u_{\mathfrak{a}_1}(t)u_{\mathfrak{a}_2}(t)u_{\mathfrak{a}_3}(t)$ (*see Fig.* 11).

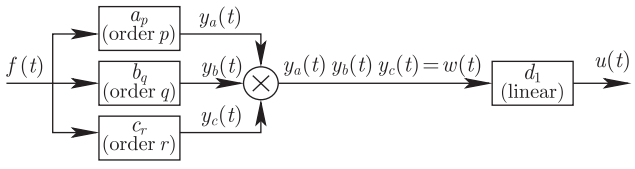

Fig. 10. Elementary ternary Volterra system of homogeneous order $n = p + q + r$.

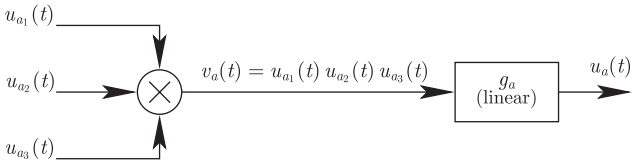

Fig. 11. Realization of $u_{\mathfrak{a}}$ for $\mathfrak{a} = (\mathfrak{a}_1, \mathfrak{a}_2, \mathfrak{a}_3) \in \mathbb{A}_n$ with odd $n \geqslant 3$: $g_{\mathfrak{a}}$ is the convolution kernel of the filter associated to the transfer function $G_{\mathfrak{a}}$.

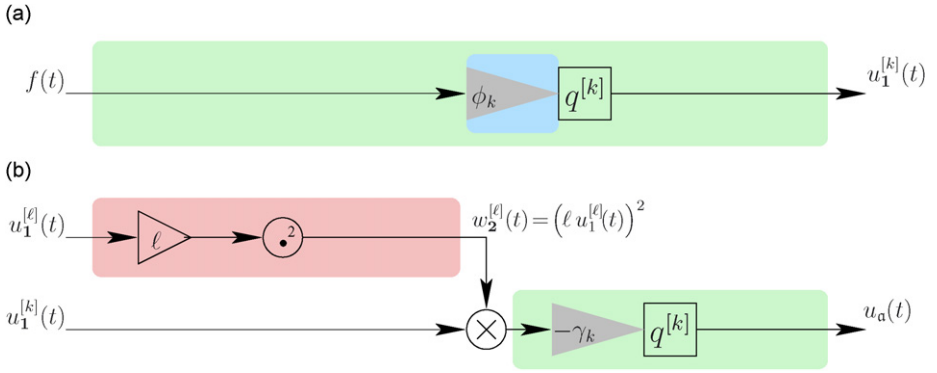

Fig. 12. (a): Realization of $u_1^{[k]}$; (b): realization of $u_{\mathfrak{a}}$ with $\mathfrak{a} = (\ell, \ell, k) \in \widetilde{\mathbb{A}}_3$.

Proof. The identification is straightforward if $n = 1$ or if n is even. Now, let $n \geqslant 3$ be odd. Let $\mathfrak{a} = (\mathfrak{a}_1, \mathfrak{a}_2, \mathfrak{a}_3) \in \mathbb{A}_n$. Then, $H_{\mathfrak{a}}$ (see Eq. (45)) has the form Eq. (46) with $p = \mathfrak{n}(\mathfrak{a}_1)$, $q = \mathfrak{n}(\mathfrak{a}_2)$, $r = \mathfrak{n}(\mathfrak{a}_3)$, and $A_p = H_{\mathfrak{a}_1}$, $B_q = H_{\mathfrak{a}_2}$, $C_r = H_{\mathfrak{a}_3}$, $D_1 = G_{\mathfrak{a}}$ (see Eq. (48)). The identification of the realizable structure arises from Definition 3. □

4.3.2. Application: building realizable structures for orders $n = 1, 3, 5$

In practice, the sound synthesis is performed for a finite number of modes $k \in \widetilde{\mathbb{A}}_1 = [1, K]_{\mathbb{N}}$ and a finite number N of kernels. The solution $u(x, t)$ given by Eq. (47) is approximated by

$$\breve{u}_N(x,t) = \sum_{n=1}^{N} \sum_{\mathfrak{a} \in \widetilde{\mathbb{A}}_n} u_{\mathfrak{a}}(t) e_{\mathfrak{k}(\mathfrak{a})}(x) = \sum_{n=1}^{N} \sum_{k=1}^{K} u_n^{[k]}(t) e_k(x), \tag{49}$$

with

$$u_n^{[k]}(t) = \sum_{\mathfrak{a} \in \widetilde{\mathbb{A}}_n(k)} u_{\mathfrak{a}}(t) \tag{50}$$

and

$$\widetilde{\mathbb{A}}_n(k) = \{\mathfrak{a} \in \widetilde{\mathbb{A}}_n | \mathfrak{k}(\mathfrak{a}) = k\}. \tag{51}$$

In this section, realizations of $u_n^{[k]}$ and then of $\breve{u}_N(x, t)$ are derived using Theorem 2.

For $n = 1$ and $\mathfrak{a} = k \in \widetilde{\mathbb{A}}_1 = [1, K]_{\mathbb{N}}$, $u_{\mathfrak{a}} = u_1^{[k]}$ is the output of the linear filter with kernel $h_1^{[k]} = \phi_k q^{[k]}$ fed by $f(t)$ (see Theorem 2 and Eq. (44)). The static gain ϕ_k (see Fig. 12(a)) measures how much the mode e_k is excited by the spatial distribution ϕ.

For $n = 3$, $\mathfrak{a} \in \widetilde{\mathbb{A}}_3 \subset (\widetilde{\mathbb{A}}_1)^3$ has the form $\mathfrak{a} = (\ell, \ell, k)$. From Theorem 2 and Fig. 11, $u_{\mathfrak{a}}(t)$ is the output of the linear filter with kernel $g_{\mathfrak{a}} = -\ell^2 \gamma_k q^{[k]}$ fed by $u_1^{[\ell]}(t) u_1^{[\ell]}(t) u_1^{[k]}(t)$, where γ_k denotes

$$\gamma_k = \varepsilon k^2 \pi^4. \tag{52}$$

Separating the factors depending on ℓ from those depending on k leads to the realization in Fig. 12(b).

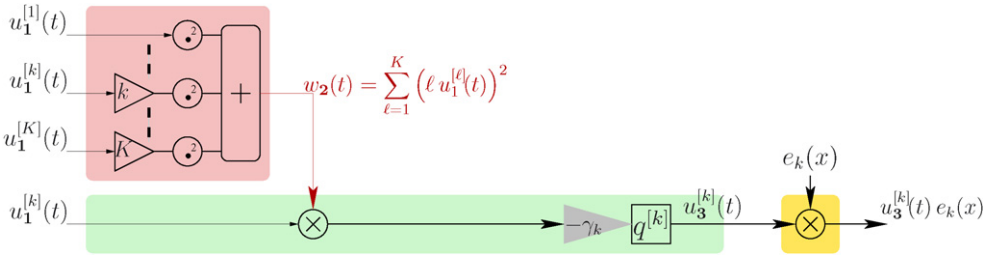

Fig. 13. Realization of $u_3^{[k]}$ with its associated modal shape $u_3^{[k]}(t)e_k(x)$.

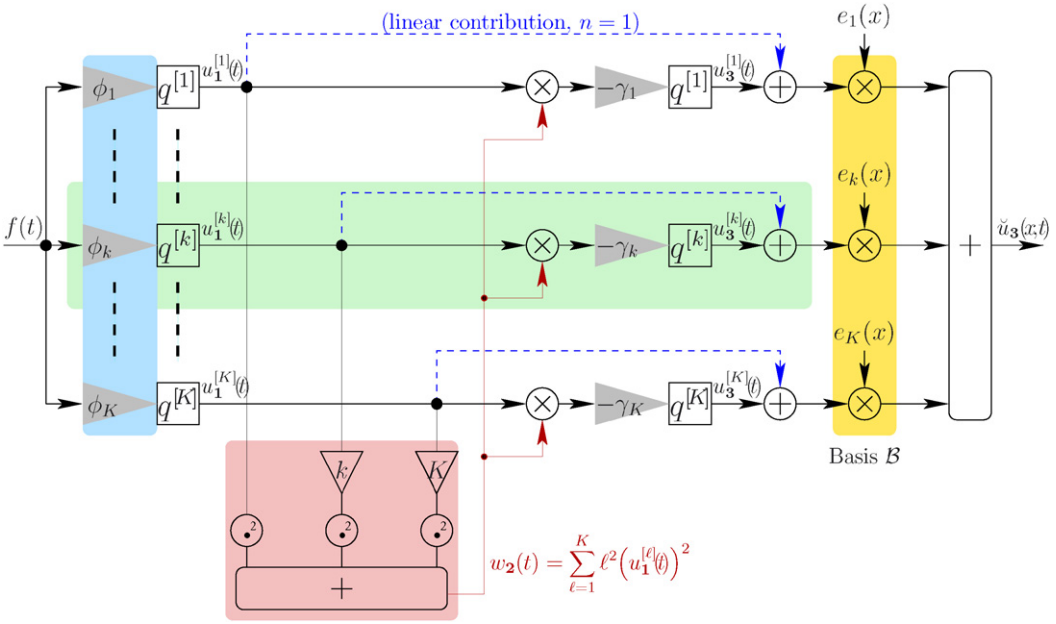

Fig. 14. Block-diagram of an $o(\varepsilon)$-simulation of (M1) with K modes: the dashed arrows isolate the linear dynamics ($n = 1$) of each mode; the shaded central part isolates the $o(\varepsilon)$-dynamics of a mode k; the shaded bottom part isolates the dynamics of the integral term in (M1) (gains 1, k and K before the square operators are due to $\partial/\partial x$); the shaded left part corresponds to simple gains, controlled by the spatial distribution of the excitation force.

The realization of $u_3^{[k]}$ ($k \in [1, K]_{\mathbb{N}}$) is obtained by summing the outputs $u_\alpha(t)$ of realizations of Fig. 12(b) over $\widetilde{\mathbb{A}}_3(k) = \{(\ell, \ell, k) | \ell \in \widetilde{\mathbb{A}}_1\}$, following Eqs. (50) and (51). Collecting all these contributions over ℓ and factorizing by the common linear filter $-\gamma_k q^{[k]}$ yield the concise realization given in Fig. 13.

As a consequence, the approximated solution $\breve{u}_3(x, t)$ in Eq. (49) can be realized as detailed in Fig. 14.

In this structure, kernels $q^{[k]}$ are the impulse responses of second-order AR-filters associated to the transfer functions $Q^{[k]}(s)$. If N_q^+ denotes the number of sums involved in a digital simulation of $q^{[k]}$ (similarly, $N_q^\times$ for products), the global complexity can be evaluated, as detailed in Table 2.

Digital implementations of linear filters involved in Fig. 14 are very standard (see e.g. Ref. [32]). Here, a method which preserves the exact eigenfrequencies and the exact dampings is proposed (see details in Appendix A.4). It leads to the parameters $N_q^+ = 4$, $N_q^\times = 5$.

Nevertheless, the products (in the time domain) of $N = 3$ signals with a frequency range $[0, f^*]$ yield a signal with frequency range $[0, Nf^\star]$. Theoretically, rejecting the aliasing due to sampling with frequency f_s requires that $f_s/2 > Nf^\star$ (Shannon–Nyquist theorem). Here, the second-order filters with impulse response $q^{[k]}$

Table 2
Number of floating point operations to compute $u(x,t)$ for (M1) with K modes, at a given time, and at N_x observation points (see Section 7 for typical values): the number of sums (N^+), products ($N^\times$), and flops ($N^{\text{flops}} = N^+ + N^\times$) are given for the linear and the third-order approximations

	Linear approx.: $N=1$, $o(\varepsilon^0)$	Third-order approx.: $N=3$, $o(\varepsilon^1)$
N^+	$K(N_q^+ + N_x) - N_x$	$K(2N_q^+ + N_x + 2) - N_x - 1$
$N^\times$	$K(N_q^\times + N_x)$	$K(2N_q^\times + N_x + 3) - 1$
N^{flops}	$K(N_q^{\text{flops}} + 2N_x) - N_x$	$K(2N_q^{\text{flops}} + 2N_x + 5) - N_x$

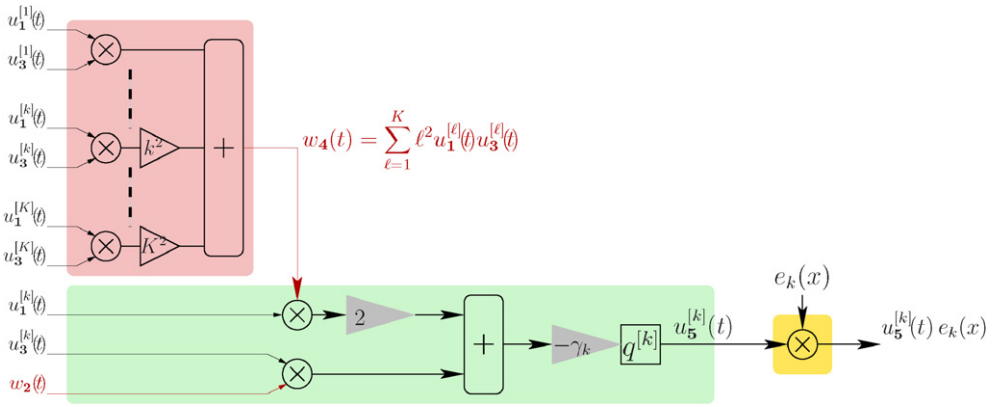

Fig. 15. Realization of $u_5^{[k]}$ with its associated modal shape $u_5^{[k]}(t)e_k(x)$.

significantly cut-off the spectrum beyond $f_k[1 + 1/Q_k]$ where the quality factor is $Q_k = k\pi/(\alpha + \beta k^2\pi^2)$. As a consequence,

$$\frac{f_s}{2} > N f_K \left(1 + \frac{1}{Q_K}\right) \tag{53}$$

is sufficient in practice. This condition will be used for the sound synthesis in Section 7.

For $n = 5$, the identification given by Theorem 2 yields the realization given in Fig. 15. Note that this structure can be also identified using Eq. (39): the first factor in Eq. (39) accounts for the filter with kernel $-\gamma_k q^{[k]}$ which is factorized in the realization (similarly to Fig. 13 for the case $n = 3$; in the second factor, the two first terms describes twice the same sub-system which corresponds to the part involving $w_4(t)$ and the gain 2 in Fig. 15; finally, the third term describes the sub-system corresponding to the bottom part involving $u_3^{[k]}(t)$ and $w_2(t)$. The realization given in Fig. 15 allows to complement Fig. 14, yielding a realization of $\breve{u}_5(x,t)$.

Numerical simulations of $\breve{u}_3$ and $\breve{u}_5$ and comparisons are presented in Section 7.

5. Solution and simulation of (M2)

Considering a string and impedance type boundary conditions defines a model which can still be solved using Volterra series (with the single input f). In this case, the kernels depend on the impedance expressions (see Ref. [31, Chapter 4]). In this section, a more general case is considered: that of a string governed by (M2) (see Eqs. (11)–(13)), and driven by three inputs which are a force f inside Ω, a displacement u_0 at $x = 0$ and a displacement u_1 at $x = 1$. This problem makes it necessary to define Volterra series for systems with three inputs, as presented in Section 5.1. The solution is derived in Section 5.2 from which a simulable structure is identified in Section 5.3.

5.1. Volterra series with three inputs

For systems with three inputs $(e_{\mathrm{I}}, e_{\mathrm{II}}, e_{\mathrm{III}})$ and one output u, the definition of Volterra series is generalized as follows:

$$\begin{aligned} u(t) = \sum_{\boldsymbol{m}\in\mathbb{M}} \int_{\mathbb{R}^{|\boldsymbol{m}|}} & h_{\boldsymbol{m}}(t^{\mathrm{I}}_{1:\boldsymbol{m}_{\mathrm{I}}}, t^{\mathrm{II}}_{1:\boldsymbol{m}_{\mathrm{II}}}, t^{\mathrm{III}}_{1:\boldsymbol{m}_{\mathrm{III}}}) e_{\mathrm{I}}(t-t^{\mathrm{I}}_1)\cdots e_{\mathrm{I}}(t-t^{\mathrm{I}}_{\boldsymbol{m}_{\mathrm{I}}}) \\ & \times e_{\mathrm{II}}(t-t^{\mathrm{II}}_1)\cdots e_{\mathrm{II}}(t-t^{\mathrm{II}}_{\boldsymbol{m}_{\mathrm{II}}}) e_{\mathrm{III}}(t-t^{\mathrm{III}}_1)\cdots e_{\mathrm{III}}(t-t^{\mathrm{III}}_{\boldsymbol{m}_{\mathrm{III}}}) \\ & \times \mathrm{d}t^{\mathrm{I}}_{1:\boldsymbol{m}_{\mathrm{I}}}\mathrm{d}t^{\mathrm{II}}_{1:\boldsymbol{m}_{\mathrm{II}}}\mathrm{d}t^{\mathrm{III}}_{1:\boldsymbol{m}_{\mathrm{III}}}, \end{aligned}$$

where the multi-index $\boldsymbol{m} = (\boldsymbol{m}_{\mathrm{I}}, \boldsymbol{m}_{\mathrm{II}}, \boldsymbol{m}_{\mathrm{III}}) \in \mathbb{M} = \mathbb{N}^3\backslash\{(0,0,0\}$ details the nonlinearity orders due to each input, while $|\boldsymbol{m}| = \boldsymbol{m}_{\mathrm{I}} + \boldsymbol{m}_{\mathrm{II}} + \boldsymbol{m}_{\mathrm{III}}$ denotes the global nonlinearity order of the kernel $h_{\boldsymbol{m}}$.

Remark 8. For a linear problem, all the kernels $h_{\boldsymbol{m}}$ are zero if $|\boldsymbol{m}| \geqslant 2$ and, possibly non-zero if $|\boldsymbol{m}| = 1$. In this case, the three available index $\boldsymbol{m} \in \{(1,0,0);(0,1,0);(0,0,1)\}$ define the solution as a superposition of three linear contributions: it leads to the standard superposition principle.

Interconnection laws Eqs. (18)–(20) become, respectively, for all $\boldsymbol{m} \in \mathbb{M}$,

$$C_{\boldsymbol{m}}(s_{\mathbf{1}:\boldsymbol{m}}) = A_{\boldsymbol{m}}(s_{\mathbf{1}:\boldsymbol{m}}) + B_{\boldsymbol{m}}(s_{\mathbf{1}:\boldsymbol{m}}), \tag{54}$$

$$C_{\boldsymbol{m}}(s_{\mathbf{1}:\boldsymbol{m}}) = \sum_{(\boldsymbol{p},\boldsymbol{q})\in\mathbb{M}^2 \text{ s.t. } \boldsymbol{p}+\boldsymbol{q}=\boldsymbol{m}} A_{\boldsymbol{p}}(s_{\mathbf{1}:\boldsymbol{p}}) B_{\boldsymbol{q}}(s_{\boldsymbol{p}+\mathbf{1}:\boldsymbol{m}}) \tag{55}$$

$$C_{\boldsymbol{m}}(s_{\mathbf{1}:\boldsymbol{m}}) = A_{\boldsymbol{m}}(s_{\mathbf{1}:\boldsymbol{m}}) B_1(\widehat{s_{\mathbf{1}:\boldsymbol{m}}}). \tag{56}$$

with the notations $\mathbf{1} = (1,1,1)$, $\boldsymbol{p}+\boldsymbol{q} = (\boldsymbol{p}_{\mathrm{I}}+\boldsymbol{q}_{\mathrm{I}}, \boldsymbol{p}_{\mathrm{II}}+\boldsymbol{q}_{\mathrm{II}}, \boldsymbol{p}_{\mathrm{III}}+\boldsymbol{q}_{\mathrm{III}})$ for $(\boldsymbol{p},\boldsymbol{q}) \in \mathbb{M}^2$ and, if $\boldsymbol{p} \leqslant \boldsymbol{q}$ (that is $\boldsymbol{p}_{\mathrm{I}} \leqslant \boldsymbol{q}_{\mathrm{I}}$, $\boldsymbol{p}_{\mathrm{II}} \leqslant \boldsymbol{q}_{\mathrm{II}}$, $\boldsymbol{p}_{\mathrm{III}} \leqslant \boldsymbol{q}_{\mathrm{III}}$),

$$(s_{\boldsymbol{p}:\boldsymbol{q}}) = (s^{\mathrm{I}}_{\boldsymbol{p}_{\mathrm{I}}}, s^{\mathrm{I}}_{\boldsymbol{p}_{\mathrm{I}}+1}, \ldots, s^{\mathrm{I}}_{\boldsymbol{q}_{\mathrm{I}}}, s^{\mathrm{II}}_{\boldsymbol{p}_{\mathrm{II}}}, s^{\mathrm{II}}_{\boldsymbol{p}_{\mathrm{II}}+1}, \ldots, s^{\mathrm{II}}_{\boldsymbol{q}_{\mathrm{II}}}, s^{\mathrm{III}}_{\boldsymbol{p}_{\mathrm{III}}}, s^{\mathrm{III}}_{\boldsymbol{p}_{\mathrm{III}}+1}, \ldots, s^{\mathrm{III}}_{\boldsymbol{q}_{\mathrm{III}}}), \tag{57}$$

$$\widehat{s_{\boldsymbol{p}:\boldsymbol{q}}} = s^{\mathrm{I}}_{\boldsymbol{p}_{\mathrm{I}}} + s^{\mathrm{I}}_{\boldsymbol{p}_{\mathrm{I}}+1} + \cdots + s^{\mathrm{I}}_{\boldsymbol{q}_{\mathrm{I}}} + s^{\mathrm{II}}_{\boldsymbol{p}_{\mathrm{II}}} + s^{\mathrm{II}}_{\boldsymbol{p}_{\mathrm{II}}+1} + \cdots + s^{\mathrm{II}}_{\boldsymbol{q}_{\mathrm{II}}} + s^{\mathrm{III}}_{\boldsymbol{p}_{\mathrm{III}}} + s^{\mathrm{III}}_{\boldsymbol{p}_{\mathrm{III}}+1} + \cdots + s^{\mathrm{III}}_{\boldsymbol{q}_{\mathrm{III}}}. \tag{58}$$

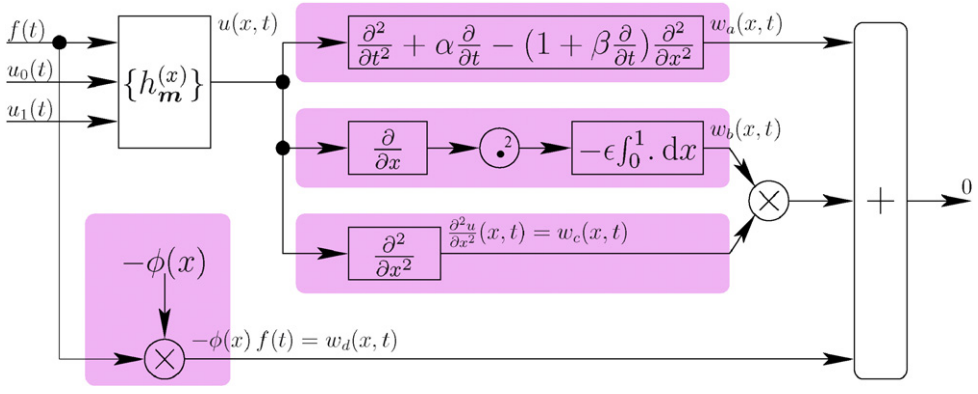

Fig. 16. Block-diagram representing Eq. (11).

5.2. Derivation of the Volterra kernels for (M2)

Modelling the displacement $u(x,t)$ using a Volterra series $\{h_m^{(x)}\}_{m\in\mathbb{M}}$ with inputs $e_{\rm I}(t)=f(t)$, $e_{\rm II}(t)=u_0(t)$, $e_{\rm III}(t)=u_1(t)$ and translating Eq. (11) into the block-diagram in Fig. 16 allow to derive the following equation through Eqs. (54)–(56): for all $\boldsymbol{m}\in\mathbb{M}$ and $(x,s_{\mathbf{1}:\boldsymbol{m}})\in\Omega\times(\mathbb{C}_0^+)^{|\boldsymbol{m}|}$,

$$[\Gamma(\widehat{s_{\mathbf{1}:\boldsymbol{m}}})]^2 H_{\boldsymbol{m}}^{(x)}(s_{\mathbf{1}:\boldsymbol{m}})-\frac{\partial^2 H_{\boldsymbol{m}}^{(x)}(s_{\mathbf{1}:\boldsymbol{m}})}{\partial x^2}=\frac{E_{\boldsymbol{m}}^{(x)}(s_{\mathbf{1}:\boldsymbol{m}})}{1+\beta\widehat{s_{\mathbf{1}:\boldsymbol{m}}}},\tag{59}$$

with

$$E_{\boldsymbol{m}}^{(x)}(s_1^{\rm I})=\phi(x)\quad\text{if }\boldsymbol{m}=(1,0,0),\tag{60}$$

$$E_{\boldsymbol{m}}^{(x)}(s_1^{\rm II})=0\quad\text{if }\boldsymbol{m}=(0,1,0),\tag{61}$$

$$E_{\boldsymbol{m}}^{(x)}(s_1^{\rm III})=0\quad\text{if }\boldsymbol{m}=(0,0,1),\tag{62}$$

$$E_{\boldsymbol{m}}^{(x)}(s_{\mathbf{1}:\boldsymbol{m}})=\varepsilon\sum_{\substack{(\boldsymbol{p},\boldsymbol{q},\boldsymbol{r})\in\mathbb{M}^3\\ \boldsymbol{p}+\boldsymbol{q}+\boldsymbol{r}=\boldsymbol{m}}}\int_0^1\left[\frac{\partial H_{\boldsymbol{p}}^{(x)}(s_{\mathbf{1}:\boldsymbol{p}})}{\partial x}\frac{\partial H_{\boldsymbol{q}}^{(x)}(s_{\boldsymbol{p}+\mathbf{1}:\boldsymbol{p}+\boldsymbol{q}})}{\partial x}\right]\mathrm{d}x\,\frac{\partial^2 H_{\boldsymbol{r}}^{(x)}(s_{\boldsymbol{p}+\boldsymbol{q}+\mathbf{1}:\boldsymbol{m}})}{\partial x^2}\quad\text{if }|\boldsymbol{m}|\geqslant 2.\tag{63}$$

The boundary conditions Eq. (12) translate into, for all $\boldsymbol{m}\in\mathbb{M}$ and $(s_{\mathbf{1}:\boldsymbol{m}})\in(\mathbb{C}_0^+)^{|\boldsymbol{m}|}$,

$$[H_{\boldsymbol{m}}^{(x=0)}(s_1^{\rm II}),H_{\boldsymbol{m}}^{(x=1)}(s_1^{\rm II})]=[1,0]\quad\text{if }\boldsymbol{m}=(0,1,0),\tag{64}$$

$$[H_{\boldsymbol{m}}^{(x=0)}(s_1^{\rm III}),H_{\boldsymbol{m}}^{(x=1)}(s_1^{\rm III})]=[0,1]\quad\text{if }\boldsymbol{m}=(0,0,1),\tag{65}$$

$$[H_{\boldsymbol{m}}^{(x=0)}(s_{\mathbf{1}:\boldsymbol{m}}),H_{\boldsymbol{m}}^{(x=1)}(s_{\mathbf{1}:\boldsymbol{m}})]=[0,0]\quad\text{if }\boldsymbol{m}=(1,0,0)\text{ or }|\boldsymbol{m}|\geqslant 2.\tag{66}$$

For each $\boldsymbol{m}\in\mathbb{M}$, Eqs. (59)–(66), define a second-order linear boundary value problem which can be solved analytically, or through a decomposition on a basis, as in Section 4.2. Similarly to (M1), kernels $H_{\boldsymbol{m}}^{(x)}$ are zero for even $|\boldsymbol{m}|$.

More precisely, exact expressions of $H_{\boldsymbol{m}}^{(x)}$ are given by, for all $\boldsymbol{m}\in\mathbb{M}$, $(s_{\mathbf{1}:\boldsymbol{m}})\in(\mathbb{C}_0^+)^{|\boldsymbol{m}|}$ and using the definitions Eqs. (25) and (28)

$$H_{\boldsymbol{m}}^{x}s_1^{\rm II}=\sinh((1-x)\Gamma(s_1^{\rm II}))/\sinh\Gamma(s_1^{\rm II})\quad\text{if }\boldsymbol{m}=(0,1,0),\tag{67}$$

$$H_{\boldsymbol{m}}^{(x)}(s_1^{\rm III})=\sinh(x\Gamma(s_1^{\rm III}))/\sinh\Gamma(s_1^{\rm III})\quad\text{if }\boldsymbol{m}=(0,0,1),\tag{68}$$

$$H_{\boldsymbol{m}}^{(x)}(s_{\mathbf{1}:\boldsymbol{m}})=\int_\Omega G(x,\xi,\widehat{s_{\mathbf{1}:\boldsymbol{m}}})E_{\boldsymbol{m}}^{(\xi)}(s_{\mathbf{1}:\boldsymbol{m}})\,\mathrm{d}\xi\quad\text{if }\boldsymbol{m}=(1,0,0)\text{ or }|\boldsymbol{m}|\geqslant 2.\tag{69}$$

The functions $e_k\in\mathscr{B}$ are the eigenfunctions of the problems Eqs. (59)–(66) if $\boldsymbol{m}=\{(1,0,0\}$ or $|\boldsymbol{m}|\geqslant 2$. The cases $\boldsymbol{m}\in\{(0,1,0);(0,0,1)\}$ are associated to two distinct bases of eigenfunctions, even if $\mathscr{B}$ still defines an L^2-orthogonal basis. A decomposition on a L^2-basis ensures the convergence towards the solution for the quadratic mean but not necessarily at a given location x: this is the so-called Gibbs' effect. It will be precisely the case at $x=0$ and 1, if we choose $\mathscr{B}$ for $\boldsymbol{m}\in\{(0,1,0);(0,0,1)\}$. Nevertheless, this choice simplifies the derivation of solutions. It yields the following results, using the definition Eq. (34), for all $\boldsymbol{m}\in\mathbb{M}$, $k\in\mathbb{N}^*$, $(s_{\mathbf{1}:\boldsymbol{m}})\in(\mathbb{C}_0^+)^{|\boldsymbol{m}|}$,

$$H_{\boldsymbol{m}}^{(x)}(s_{\mathbf{1}:\boldsymbol{m}})\underset{L^2}{=}\sum_{k\in\mathbb{N}^*}H_{\boldsymbol{m}}^{[k]}(s_{\mathbf{1}:\boldsymbol{m}})e_k(x),\tag{70}$$

$$H_{\boldsymbol{m}}^{[k]}(s_1^{\rm I})=\phi_k Q^{[k]}(s_1^{\rm I})\quad\text{if }\boldsymbol{m}=(1,0,0),\tag{71}$$

$$H_{\boldsymbol{m}}^{[k]}(s_1^{\rm II})=\sqrt{2}k\pi(1+\beta s_1^{\rm II})Q^{[k]}(s_1^{\rm II})\quad\text{if }\boldsymbol{m}=(0,1,0),\tag{72}$$

$$H_{\boldsymbol{m}}^{[k]}(s_1^{\mathrm{III}}) = (-1)^{k+1}\sqrt{2}k\pi(1+\beta s_1^{\mathrm{III}})Q^{[k]}(s_1^{\mathrm{III}}) \quad \text{if } \boldsymbol{m}=(0,0,1), \tag{73}$$

$$H_{\boldsymbol{m}}^{[k]}(s_{\mathbf{1}:\boldsymbol{m}}) = -\varepsilon k^2\pi^4 Q^{[k]}(\widehat{s_{\mathbf{1}:\boldsymbol{m}}}) \sum_{\substack{(\boldsymbol{p},\boldsymbol{q},\boldsymbol{r})\in\mathbb{M}^3\\ \boldsymbol{p}+\boldsymbol{q}+\boldsymbol{r}=\boldsymbol{m}}} \left[\sum_{\ell\in\mathbb{N}^*} \ell^2 H_{\boldsymbol{p}}^{[\ell]}(s_{\mathbf{1}:\boldsymbol{p}}) H_{\boldsymbol{q}}^{[\ell]}(s_{\boldsymbol{p}+\mathbf{1}:\boldsymbol{p}+\boldsymbol{q}})\right]$$
$$\times H_{\boldsymbol{r}}^{[k]}(s_{\boldsymbol{p}+\boldsymbol{q}+\mathbf{1}:\boldsymbol{m}}) \quad \text{if } |\boldsymbol{m}|\geqslant 2. \tag{74}$$

The combinatorics can be still organized as one sum of elementary terms, as follows.

Theorem 3. *Let $\mathbb{B}_{\boldsymbol{m}}$ be the sets of full ternary trees defined by, for $\boldsymbol{m}\in\mathbb{M}$,*

$$\mathbb{B}_{(1,0,0)}=\mathbb{N}^*\times\{\mathrm{I}\}, \mathbb{B}_{(0,1,0)}=\mathbb{N}^*\times\{\mathrm{II}\}, \mathbb{B}_{(0,0,1)}=\mathbb{N}^*\times\{\mathrm{III}\} \quad \textit{if } |\boldsymbol{m}|=1, \tag{75}$$

$$\mathbb{B}_{\boldsymbol{m}}=\emptyset \quad \textit{if } |\boldsymbol{m}| \textit{ is even}, \tag{76}$$

$$\mathbb{B}_{\boldsymbol{m}} = \bigcup_{\substack{(\boldsymbol{p},\boldsymbol{q},\boldsymbol{r})\in\mathbb{M}^3\\ |\boldsymbol{p}|,|\boldsymbol{q}|,|\boldsymbol{r}| \textit{ odd}\\ \boldsymbol{p}+\boldsymbol{q}+\boldsymbol{r}=\boldsymbol{m}}} \{(\mathfrak{b}_1,\mathfrak{b}_2,\mathfrak{b}_3)\in\mathbb{B}_{\boldsymbol{p}}\times\mathbb{B}_{\boldsymbol{q}}\times\mathbb{B}_{\boldsymbol{r}} / \mathfrak{f}(\mathfrak{b}_1)=\mathfrak{f}(\mathfrak{b}_2)\} \quad \textit{if } |\boldsymbol{m}|\geqslant 3 \textit{ is odd}, \tag{77}$$

where, for all $\boldsymbol{m}\in\mathbb{M}$ and $\mathfrak{b}\in\mathbb{B}_{\boldsymbol{m}}$, the definition of $\mathfrak{f}(\mathfrak{b})$ is the following: if $|\boldsymbol{m}|=1$ so that $\mathfrak{b}=(k,\imath)\in\mathbb{N}^*\times\{\mathrm{I},\mathrm{II},\mathrm{III}\}$, then $\mathfrak{f}(\mathfrak{b})=k$; if $|\boldsymbol{m}|\geqslant 3$ is odd so that $\mathfrak{b}=(\mathfrak{b}_1,\mathfrak{b}_2,\mathfrak{b}_3)$, then $\mathfrak{f}(\mathfrak{b})=\mathfrak{f}(\mathfrak{b}_3)$.

Then, for all $\boldsymbol{m}\in\mathbb{M}$, kernels $H_{\boldsymbol{m}}^{(x)}$ are given by, for all $(x,s_{\mathbf{1}:\boldsymbol{m}})\in\Omega\times(\mathbb{C}_0^+)^{|\boldsymbol{m}|}$,

$$H_{\boldsymbol{m}}^{(x)}(s_{\mathbf{1}:\boldsymbol{m}}) = \sum_{\mathfrak{b}\in\mathbb{B}_{\boldsymbol{m}}} H_{\mathfrak{b}}(s_{\mathbf{1}:\boldsymbol{m}}) e_{\mathfrak{f}(\mathfrak{b})}(x), \tag{78}$$

where, for all $\mathfrak{b}\in\mathbb{B}_{\boldsymbol{m}}$ (with $|\boldsymbol{m}|$ odd and $\mathfrak{b}=(\mathfrak{b}_1,\mathfrak{b}_2,\mathfrak{b}_3)$ if $|\boldsymbol{m}|\geqslant 3$),

$$\textit{if } |\boldsymbol{m}|=1, \quad H_{\mathfrak{b}}=H_{\boldsymbol{m}}^{[\mathfrak{f}(\mathfrak{b})]}, \quad (\textit{see Eqs. } (71)-(73)) \tag{79}$$

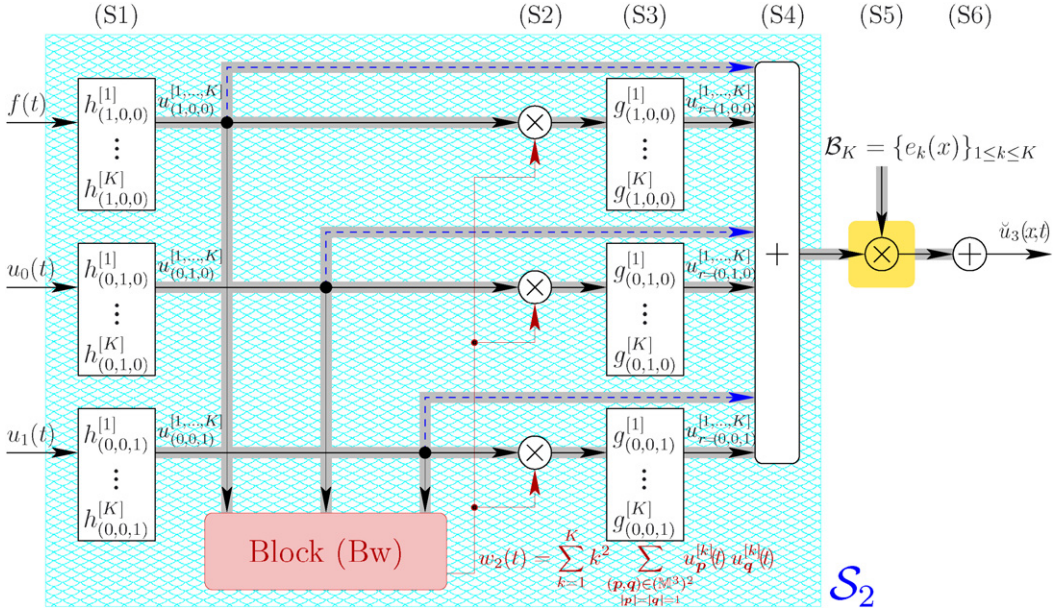

Fig. 17. Block-diagram of an $o(\varepsilon)$-simulation of (M2) with K modes: the shaded arrows carry vectors composed of K signals while the non-shaded ones carry only 1 signal. The first stage (S1) corresponds to three filter-banks of dimension K. The first filter-bank is fed by the force $f(t)$, second one by $u_0(t)$ and the third one by $u_1(t)$. The block (Bw) is described in Fig. 18. The stage (S2) corresponds to the multiplications of a vector signal by a scalar signal in the time domain and (S3) to $3K$-filters, each filter being fed by one signal. The stage (S4) adds six K-dimensional vectors. Then, outside the structure $\mathscr{S}_2$, the stage (S5) multiplies (for each coordinate, separately) the coordinates of two K-dimensional vector, before being added in (S6).

$$\text{if } |\boldsymbol{m}|\geqslant 3,\quad H_{\mathfrak{b}}(s_{\mathbf{1}:\boldsymbol{m}}) = -\varepsilon[\mathfrak{k}(\mathfrak{b}_1)\mathfrak{k}(\mathfrak{b}_3)\pi^2]^2 Q^{[\mathfrak{k}(\mathfrak{b})]}(\widehat{s_{\mathbf{1}:\boldsymbol{m}}})H_{\mathfrak{b}_1}(s_{\mathbf{1}:\mathfrak{m}(\mathfrak{b}_1)}) \times H_{\mathfrak{b}_2}(s_{\mathfrak{m}(\mathfrak{b}_1)+\mathbf{1}:\mathfrak{m}(\mathfrak{b}_1)+\mathfrak{m}(\mathfrak{b}_2)})H_{\mathfrak{b}_3}(s_{\mathfrak{m}(\mathfrak{b}_1)+\mathfrak{m}(\mathfrak{b}_2)+\mathbf{1}:\boldsymbol{m}}), \tag{80}$$

where $\mathfrak{m}(\mathfrak{b}) = (\boldsymbol{m}_{\mathrm{I}}, \boldsymbol{m}_{\mathrm{II}}, \boldsymbol{m}_{\mathrm{III}}) = \boldsymbol{m}$ *counts the number of leaves which are labelled by* I, II *and* III, *respectively*.

5.3. Identification of a simulable structure and connection to a bridge

An identification in Eqs. (70)–(74) for $|\boldsymbol{m}|\leqslant 3$ and a finite number of modes ($1\leqslant k\leqslant K$) leads to the structure presented in Fig. 17, which gives an $o(\varepsilon)$-approximation of the solution.

In this figure, $h_{\boldsymbol{m}}^{[k]}$ are linear filters (see Eqs. (71)–(73)). Their simulation can be performed as for $q^{[k]}$ (see Appendix A.4) with $\mathbf{C} = \phi_k[1,0]$ for $\boldsymbol{m} = (1,0,0)$, with $\mathbf{C} = \sqrt{2}k\pi[1,\beta]$ for $\boldsymbol{m} = (0,1,0)$, and with $\mathbf{C} = (-1)^{k+1}\sqrt{2}k\pi[1,\beta]$ for $\boldsymbol{m} = (0,0,1)$. This is also the case for $g_{\boldsymbol{m}}^{[k]} = -\gamma_k q^{[k]}$ (see Eq. (52)) which can be performed with $\mathbf{C} = -\gamma_k[1,0]$ for $|\boldsymbol{m}| = 1$. Thus, all the filters of this structure have the same complexity, namely, $N_h^+ = N_g^+ = 4$ and $N_h^\times = N_g^\times = 5$. The global complexity for a discrete-time realization of this structure with the optimized version of (Bw) presented in Fig. 18 (right) is detailed in Table 3.

Remark. Choosing $\mathscr{D}_K = \{\partial e_k/\partial x(x)\}_{1\leqslant k\leqslant K}$ in place of $\mathscr{B}_K = \{e_k(x)\}_{1\leqslant k\leqslant K}$ computes the output $\partial u_3/\partial x(x,t)$. Thus, at $x = 0$ or 1, this makes it possible the structure to be connected to other systems at the boundaries,

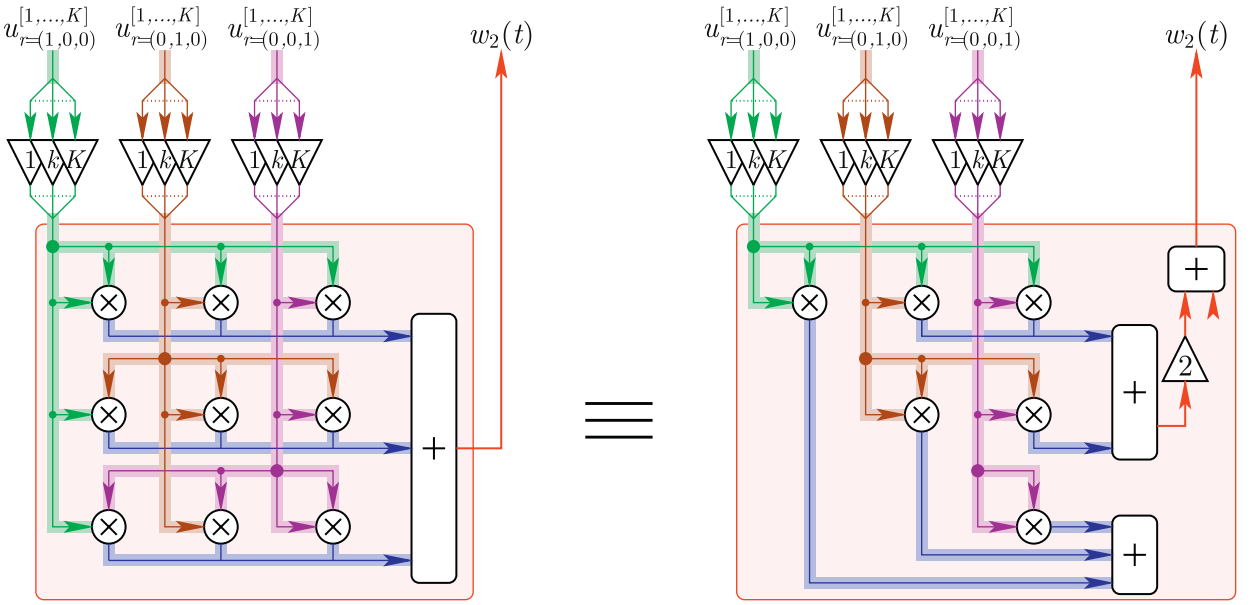

Fig. 18. Detailed block-diagram of (Bw): the products act on each coordinates separately while sums add all the signals (all coordinates of all vectors).

Table 3
Number of floating point operations to compute $u(x,t)$ for (M2) with K modes, at a given time and at N_x distinct locations for (M2): N_h^+ denotes the number of sums involved in the simulation of a filter $h_1^{[k]}$ ($N_h^\times$ for products and N_g^+,$N_g^\times$ for $g_1^{[k]}$)

	Linear approx.: $N = 1$, $o(\varepsilon^0)$	Third-order approx.: $N = 3$, $o(\varepsilon^1)$
N^+	$K(3N_h^+ + N_x + 2) - N_x$	$K(3N_h^+ + 3N_g^+ + N_x + 10) - N_x - 1$
$N^\times$	$K(3N_h^\times + N_x)$	$K(3N_h^\times + 3N_g^\times + N_x + 12) - 2$
N^{flops}	$K(3N_h^{\text{flops}} + 2N_x + 2) - N_x$	$K(6N_h^{\text{flops}} + 2N_x + 22) - N_x - 3$

such as a bridge. Note that $\partial e_k/\partial x(x) = \sqrt{2}k\pi(-1)^{kx}$ for $x \in \{0,1\}$ and that the convergence holds at these points when $K \to \infty$.

6. Third model

In this section, the string is supposed to be governed by (M3) (see Eqs. (14)–(16)). The resolution is performed similarly to Section 4.

6.1. Cancelling system

No equation on the Volterra kernels can be straightforwardly derived from Eq. (14) and interconnection laws Eqs. (18)–(20), because of the square-root in Eq. (14).

Nevertheless, the Volterra kernels $\{h_n\}$ of a nonlinear system $\mathscr{S}$ and those $\{\tilde{h}_n\}$ of $\mathscr{S}_N$ (system $\mathscr{S}$ for which the nonlinearity is approximated by its Taylor expansion until order N) are the same for $n \leqslant N$.

Thus, to obtain results valid at order $N = 3$, a third-order expansion of (M3) is sufficient and corresponds to the approximation

$$\frac{\partial}{\partial x}\left[\frac{(1-(2\varepsilon/\eta))(\partial u/\partial x)}{\sqrt{1+\eta(\partial u/\partial x)^2}} + \frac{2\varepsilon}{\eta}\frac{\partial u}{\partial x}\right] \approx \frac{\partial}{\partial x}\left[\frac{\partial u}{\partial x} + \zeta\left(\frac{\partial u}{\partial x}\right)^3\right],$$

with $\zeta = \varepsilon - (\eta/2) = 2.27 \times 10^{-4}$, from which the cancelling system described in Fig. 19 is derived.

The kernels $\{H_n^{(x)}\}$ which correspond to this cancelling system, with the boundary conditions (B1), are solution of Eqs. (22), (23) and (26). Moreover, if $n \geqslant 2$, then, for all $(x, s_{1:n}) \in \Omega \times (\mathbb{C}_0^+)^n$,

$$E_n^{(x)}(s_{1:n}) = \zeta\frac{\partial}{\partial x}\left[\sum_{\substack{(p_{1:3})\in(\mathbb{N}^*)^3 \\ p_1+p_2+p_3=n}} \frac{\partial H_{p_1}^{(x)}(s_{1:p_1})}{\partial x}\frac{\partial H_{p_2}^{(x)}(s_{p_1+1:p_1+p_2})}{\partial x}\frac{\partial H_{p_3}^{(x)}(s_{p_1+p_2+1:n})}{\partial x}\right], \tag{81}$$

so that analytical solutions can still be derived using Eqs. (27) and (28).

The modal decomposition yields Eqs. (29)–(32) and, if $n \geqslant 2$, for all $(k, s_{1:n}) \in \mathbb{N}^* \times (\mathbb{C}_0^+)^n$,

$$E_n^{[k]}(s_{1:n}) = -\zeta \sum_{\substack{(p_{1:3})\in(\mathbb{N}^*)^3 \\ p_1+p_2+p_3=n}} \sum_{(k_{1:3})\in(\mathbb{N}^*)^3} \psi_{k_{1:3}}^{[k]} H_{p_1}^{[k_1]}(s_{1:p_1}) H_{p_2}^{[k_2]}(s_{p_1+1:p_1+p_2}) H_{p_3}^{[k_3]}(s_{p_1+p_2+1:n}), \tag{82}$$

with

$$\psi_{k_{1:3}}^{[k]} = -\left\langle \frac{\partial}{\partial x}\left(\frac{\partial e_{k_1}}{\partial x}\frac{\partial e_{k_2}}{\partial x}\frac{\partial e_{k_3}}{\partial x}\right), e_k \right\rangle = \frac{k_1 k_2 k_3 k \pi^4}{2}\lambda_{k_{1:3}}^{[k]}, \tag{83}$$

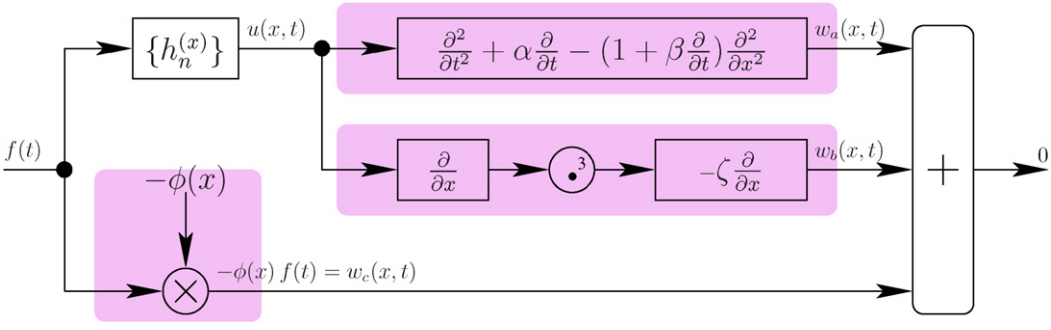

Fig. 19. Cancelling system for the third-order approximation of (M3).

and

$$\lambda^{[k]}_{k_{1:3}} = \sum_{\xi_{2:3}\in\{-1;1\}^2} \delta_{|k_1+\xi_2 k_2+\xi_3 k_3|,k}, \tag{84}$$

so that, in Eq. (82), the sum over $(k_{1:3}) \in (\mathbb{N}^*)^3$ is infinite but sparse.

This combinatorics can be organized as one sum of (non-zero) elementary terms, as follows.

Theorem 4. *Let $\mathbb{E}_n$ be the sets of full ternary trees defined by, for $n \in \mathbb{N}^*$,*

$$\mathbb{E}_1 = \mathbb{N}^*, \tag{85}$$

$$\mathbb{E}_n = \emptyset \quad \text{if } n \text{ is even}, \tag{86}$$

$$\mathbb{E}_n = \bigcup_{\substack{(p_{1:3})\in(\mathbb{N}^*)^3 \\ p_{1:3}\ odd \\ p_1+p_2+p_3=n}} \{\mathfrak{e} = (\mathfrak{e}_1, \mathfrak{e}_2, \mathfrak{e}_3, \xi_{2:3}) \in \mathbb{E}_{p_1} \times \mathbb{E}_{p_2} \times \mathbb{E}_{p_3} \times \{-1;1\}^2\} \quad \text{if } n\geqslant 3 \text{ is odd}, \tag{87}$$

where $\mathfrak{k}(\mathfrak{e}) = \mathfrak{e}$ if $\mathfrak{e} \in \mathbb{E}_1$, $\mathfrak{k}(\mathfrak{e}) = |\mathfrak{k}(\mathfrak{e}_1) + \xi_2\mathfrak{k}(\mathfrak{e}_2) + \xi_3\mathfrak{k}(\mathfrak{e}_3)|$ if $\mathfrak{e} = (\mathfrak{e}_1, \mathfrak{e}_2, \mathfrak{e}_3, \xi_{2:3}) \in \mathbb{E}_n$ with $n\geqslant 3$ and $\mathfrak{n}(\mathfrak{e}) = n$ counts the number of leaves.

Then, for all $n \in \mathbb{N}^*$, kernels $H^{(x)}_n$ are given by, for all $(x, s_{1:n}) \in \Omega \times (\mathbb{C}^+_0)^n$,

$$H^{(x)}_n(s_{1:n}) = \sum_{\mathfrak{e}\in\mathbb{E}_n} H_{\mathfrak{e}}(s_{1:n}) e_{\mathfrak{k}(\mathfrak{e})}(x), \tag{88}$$

where, for all $\mathfrak{e} \in \mathbb{E}_n$ (with n odd and $\mathfrak{e} = (\mathfrak{e}_1, \mathfrak{e}_2, \mathfrak{e}_3, \xi_{2:3})$ if $n\geqslant 3$),

$$\text{if } n = 1, \quad H_{\mathfrak{e}}(s_1) = H^{[\mathfrak{k}(\mathfrak{e})]}_n(s_1), \quad (\text{see Eq. (35)}) \tag{89}$$

$$\text{if } n\geqslant 3, \quad H_{\mathfrak{e}}(s_{1:n}) = -\frac{\zeta\mathfrak{k}(\mathfrak{e}_1)\mathfrak{k}(\mathfrak{e}_2)\mathfrak{k}(\mathfrak{e}_3)\mathfrak{k}(\mathfrak{e})\pi^4}{2} Q^{[\mathfrak{k}(\mathfrak{e})]}(\widehat{s_{1:n}}) H_{\mathfrak{e}_1}(s_{1:\mathfrak{n}(\mathfrak{e}_1)}) \times H_{\mathfrak{e}_2}(s_{\mathfrak{n}(\mathfrak{e}_1)+1:\mathfrak{n}(\mathfrak{e}_1)+\mathfrak{n}(\mathfrak{e}_2)}) H_{\mathfrak{e}_3}(s_{\mathfrak{n}(\mathfrak{e}_1)+\mathfrak{n}(\mathfrak{e}_2)+1:n}). \tag{90}$$

Another non-sparse reorganization of Eq. (82) is given by, if $n\geqslant 2$, for all $(k, s_{1:n}) \in \mathbb{N}^* \times (\mathbb{C}^+_0)^n$,

$$E^{[k]}_n(s_{1:n}) = -\chi_k \sum_{\substack{(p_{1:3})\in(\mathbb{N}^*)^3 \\ p_1+p_2+p_3=n}} \sum_{(k_{1:3})\in\mathbb{K}^3_k} k_1k_2k_3\lambda^{[k]}_{k_{1:3}} H^{[k_1]}_{p_1}(s_{1:p_1}) H^{[k_2]}_{p_2}(s_{p_1+1:p_1+p_2}) H^{[k_3]}_{p_3}(s_{p_1+p_2+1:n}), \tag{91}$$

where $\chi_k = \zeta k\pi^4/2$, $\mathbb{K}^3_k = \{(k_{1:3}) \in (\mathbb{N}^*)^3 | \exists(\xi_2, \xi_3) \in \{-1;+1\} || k_1 + \xi_2 k_2 + \xi_3 k_3| = k\}$ is illustrated in Fig. 20, and the weights $\lambda^{[k]}_{k_{1:3}}$ are detailed in Table 4.

Thus, for a finite number K of modes ($1\leqslant k\leqslant K$), identifying linear and third-order kernels from Eq. (91) rather than Eq. (33) leads to the structure in Fig. 21 (to be compared to Fig. 14).

In this structure, each output $v^{[k]}_3(t)$ of the block (Tw) is given by, for all $k \in \mathbb{N}^*$ and $t \in \mathbb{R}^+$,

$$v^{[k]}_3(t) = \sum_{(k_{1:3})\in\mathbb{K}^3_k\cap[1,K]^3_{\mathbb{N}}} \lambda^{[k]}_{k_{1:3}} k_1k_2k_3 u^{[1]}_{k_1}(t) u^{[1]}_{k_2}(t) u^{[1]}_{k_3}(t) \tag{92}$$

for which the combinatorics can be significantly reduced (about a factor 4) thanks to symmetric considerations. Indeed, similarly to Fig. 18 for the block (Bw), only the triangular superior part $\tilde{\mathbb{K}}^3_k$ of $\mathbb{K}^3_k$ can be preserved (see Fig. 22), with adapted weights $\tilde{\lambda}^{[k]}_{k_{1:3}}$ (see Table 4), as follows:

$$\tilde{\mathbb{K}}^3_k = \mathbb{K}^3_k \cap \{(k_{1:3}) \in [1, K]^3_{\mathbb{N}} | k_1\leqslant k_2\leqslant k_3\}, \tag{93}$$

$$\tilde{\lambda}^{[k]}_{k_{1:3}} = C_{k_{1:3}}\lambda^{[k]}_{k_{1:3}} \tag{94}$$

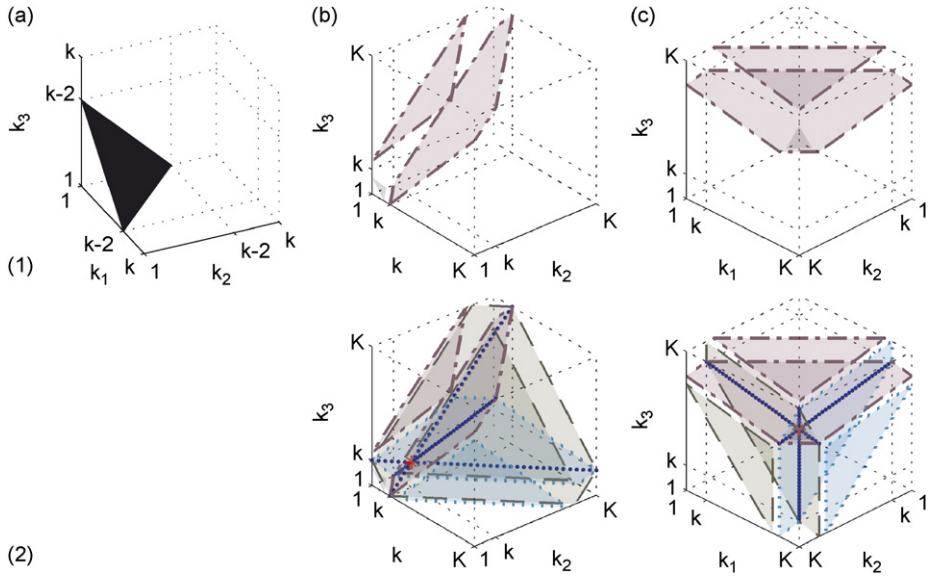

Fig. 20. The set $\mathbb{K}_k^3$ is composed of triplets of integers $(k_{1:3})$ which belong to: a triangle if $(\xi_{2:3}) = (1, 1)$ (see (1a)); a couple of semi-infinite parts of parallel planes if $(\xi_{2:3}) = (1, -1)$ (see (1b,1c)); the cases $(\xi_{2:3}) = (-1, 1)$ and $(\xi_{2:3}) = (-1, -1)$ are symmetric versions of the previous case. All the contributions are gathered in (2b,2c). Parts which are not intersected correspond to a weight $\lambda_{k_{1:3}}^{[k]} = 1$, intersections of 2 planes (blue points) to $\lambda_{k_{1:3}}^{[k]} = 2$, the intersection of three planes (one red point, $k_1 = k_2 = k_3 = k$) to $\lambda_{k_{1:3}}^{[k]} = 3$.

Table 4
Detailed weights $\lambda_{k_{1:3}}^{[k]}$ and $\tilde{\lambda}_{k_{1:3}}^{[k]}$

Cases	$\lambda_{k_{1:3}^{[k]}}$	Subcases	$C_{k_{1:3}}$	$\tilde{\lambda}_{k_{1:3}^{[k]}}$
①: $k_1 = k_2 = k_3 = k$	3	none	1	3
②: $k_1 = k_2 \neq k$ and $k_3 = k$ (and the two permutations)	2	none	3	6
③: Other cases, if $(k_{1:3}) \in \mathbb{K}_k^3$	1	ⓐ: $k_1 = k_2 = k_3 \neq k$	1	1
		ⓑ: $k_1 = k_2 \neq k_3 \neq k$ (and the two permutat.)	3	3
		ⓒ: $k_1 \neq k_2 \neq k_3 \neq k_1$	6	6
④: Other cases, if $(k_{1:3}) \notin \mathbb{K}_k^3$	0	×	×	0

with

$$C_{k_{1:3}} = \mathbf{card}\{(k_1, k_2, k_3); (k_1, k_3, k_2); (k_2, k_1, k_3); (k_3, k_1, k_2); (k_2, k_3, k_1); (k_3, k_2, k_1)\}. \tag{95}$$

The simulation of the structure in Fig. 21 involves exactly the same filters as in Fig. 14. The only difference is the block (Tw), the simulation of which is performed using Eq. (92), for each mode k and at each time.

7. Sound synthesis

In this section, we propose to simulate models (M1) and (M3) for the following parameters:

- the geometry and the physical constants are those given in Table 1.
- the excitation $\phi(x)f(t)$ is defined by, for $x \in]0, L[$ and $t \in \mathbb{R}_+^\star$

$$\phi(x) = \phi_{\max} \cos\left(\pi \frac{x - x_0}{\ell}\right) 1_{[x_0 - \frac{\ell}{2}, x_0 + \frac{\ell}{2}]}(x), \tag{96}$$

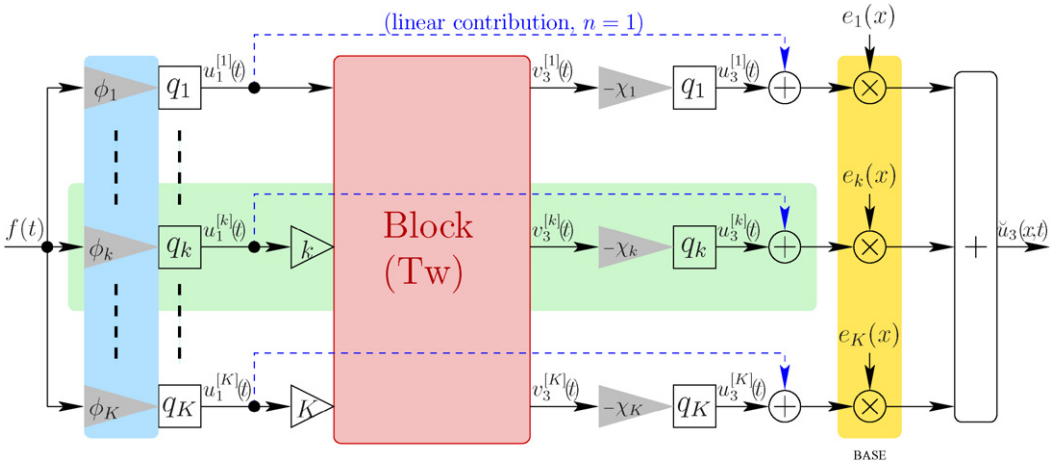

Fig. 21. Block-diagram of a $o(\varepsilon_3)$-simulation of (M3) with K modes. Each output $v_3^{[k]}(t)$ of the block (Tw) is a linear combination of products of triplets $(u_{k_1}^{[1]}(t)u_{k_2}^{[1]}(t)u_{k_3}^{[1]}(t))$ (see Eq. (92)).

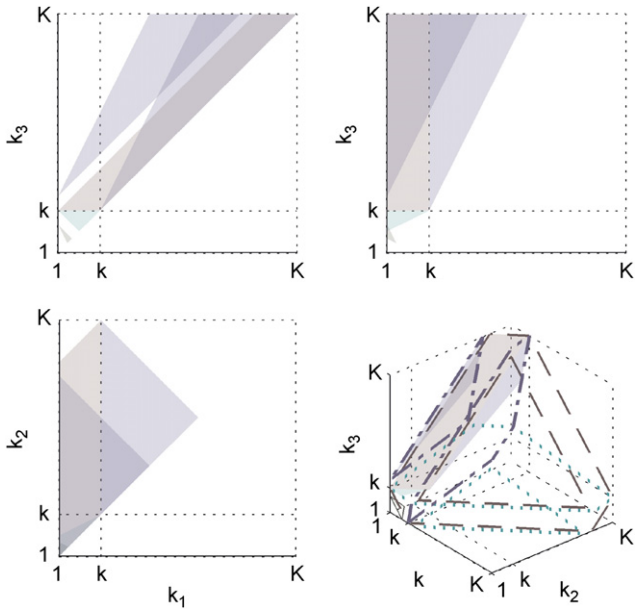

Fig. 22. Views of the set $\tilde{\mathbb{K}}_k^3$.

$$f(t) = F_{\max}\frac{t}{T}1_{[0,T]}(t), \tag{97}$$

where $x_0 = 0.63\,\mathrm{m}$, $\ell = 0.072\,\mathrm{m}$ ($\tilde{x}_0 = x_0/L = 0.35$, $\tilde{\ell} = \ell/L = 0.04$ so that 4% of string is plucked), $\phi_{\max} = \pi/(2\rho A\ell) = 395.7\,\mathrm{kg}^{-1}$ so that Eq. (1) is satisfied ($\tilde{\phi}_{\max} = \pi/(2\tilde{\ell}) = 39.27$), $T = 10\,\mathrm{ms}$ ($\tilde{T} = 1.1$). Several Forces $F_{\max}$ are used to investigate the nonlinear effects: $F_{\max}^1 = 5\,\mathrm{N}$, $F_{\max}^2 = 20\,\mathrm{N}$, $F_{\max}^3 = 40\,\mathrm{N}$, and $F_{\max}^4 = 160\,\mathrm{N}$ ($\tilde{F}_{\max}^1 = 2.8$, $\tilde{F}_{\max}^2 = 11.1$, $\tilde{F}_{\max}^3 = 22.2$, $\tilde{F}_{\max}^4 = 88.8$).

- the sampling frequency is $f_s = 44,100\,\mathrm{Hz}$ ($\tilde{f}_s = 401$), the number of modes is $K = 20$, the order of approximation is $N = 3$ in Section 7.1, and $N = 5$ in Section 7.2.

For these data, the resonance frequencies $f_k = c/L\sqrt{k^2\pi^2 - (\alpha + \beta k^2\pi^2)^2}/(2\pi)$ of the band-pass filters with kernel $q_1^{[k]}$ (see Eqs. (34) and (35)) grow from $f_1 \approx 55\,\text{Hz}$ to $f_K \approx 1100\,\text{Hz}$. The aliasing due to the nonlinearities is rejected since $N \leqslant N_{\max} = f_s/2f_K(1 + \frac{1}{Q_K})^{-1} \approx 20$ (see Eq. (53)).

7.1. Third-order approximations ($N = 3$)

Figs. 23–26 present third-order approximations $\breve{u}_3(x,t)$ of the (dimensional) displacement observed at $x = 0.57L \approx 1\,\text{m}$.

For the lowest excitation $F^1_{\max} = 5\,\text{N}$ (Fig. 23), the nonlinear contribution is negligible for both models (M1) and (M3): the spectrum of u_3 is approximately 50 dB lower than that of the linear displacement u_1. In the time domain, the maximal value of contributions u_1 and u_3 are $\max_t|u_1| \approx 0.9\,\text{mm}$ and $\max_t|u_3| < 0.012\,\text{mm}$, respectively. In this case, considering nonlinear models and using Volterra series are needless. As a matter of fact, (M1) and (M3) become equivalent since, precisely, their linear kernels $h_1^{(x)}$ are the same.

For $F^2_{\max} = 20\,\text{N}$ (Fig. 24), the nonlinear contributions u_3 begin to be significantly activated and have similar shapes for both models ((M1) and (M3)). Nevertheless, this activation is slightly more perceptible for (M3) than for (M1): while $\max_t|u_1| \approx 3.7\,\text{mm}$ (for both models), $\max_t|u_3| \approx 0.5\,\text{mm}$ for (M1) and $\max_t|u_3| \approx 0.8\,\text{mm}$ for (M3). From a qualitative point of view, it can be observed on the spectra that the eigenfrequencies are the same for the linear and the nonlinear contributions. This is because the order of the nonlinearity is odd.

For the case $F^3_{\max} = 40\,\text{N}$ (Fig. 25), contributions u_1 and u_3 have similar magnitudes (in the time domain as well as the frequency domain): $\max_t|u_1| \approx 7.4\,\text{mm}$ (for both models), $\max_t|u_3| \approx 3.84\,\text{mm}$ for (M1) and $\max_t|u_3| \approx 6.04\,\text{mm}$ for (M3). In practice, this case can be viewed as the limit of the $o(\varepsilon)$-approximation validity, and more generally, of using truncated Volterra series.

Finally, for $F^4_{\max} = 160\,\text{N}$ (Fig. 26), the nonlinear contribution u_3 are greater than the linear one for both models: $\max_t|u_1| \approx 29.5\,\text{mm}$ (for both models), $\max_t|u_3| \approx 245.7\,\text{mm}$ for (M1) and $\max_t|u_3| \approx 386.6\,\text{mm}$ for (M3). The approximation is not valid anymore.

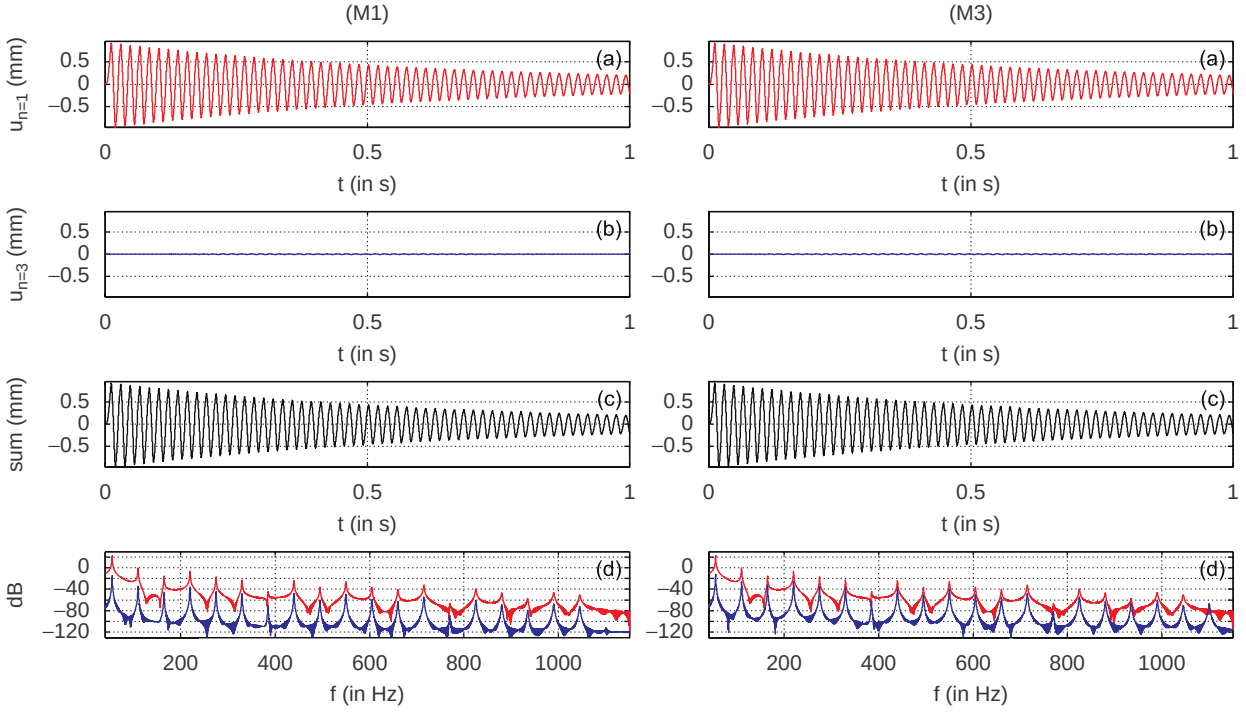

Fig. 23. Simulation of (M1) (left) and (M3) (right) for the same excitation with magnitude $F_{\max} = 5\,\text{N}$. The output u is observed at $x = 0.57L \approx 1\,\text{m}$. From top to bottom: (a) linear response, (b) output of order 3 alone, (c) sum of the linear and of the nonlinear contributions, and (d) magnitude of the spectrum of (a) and (b).

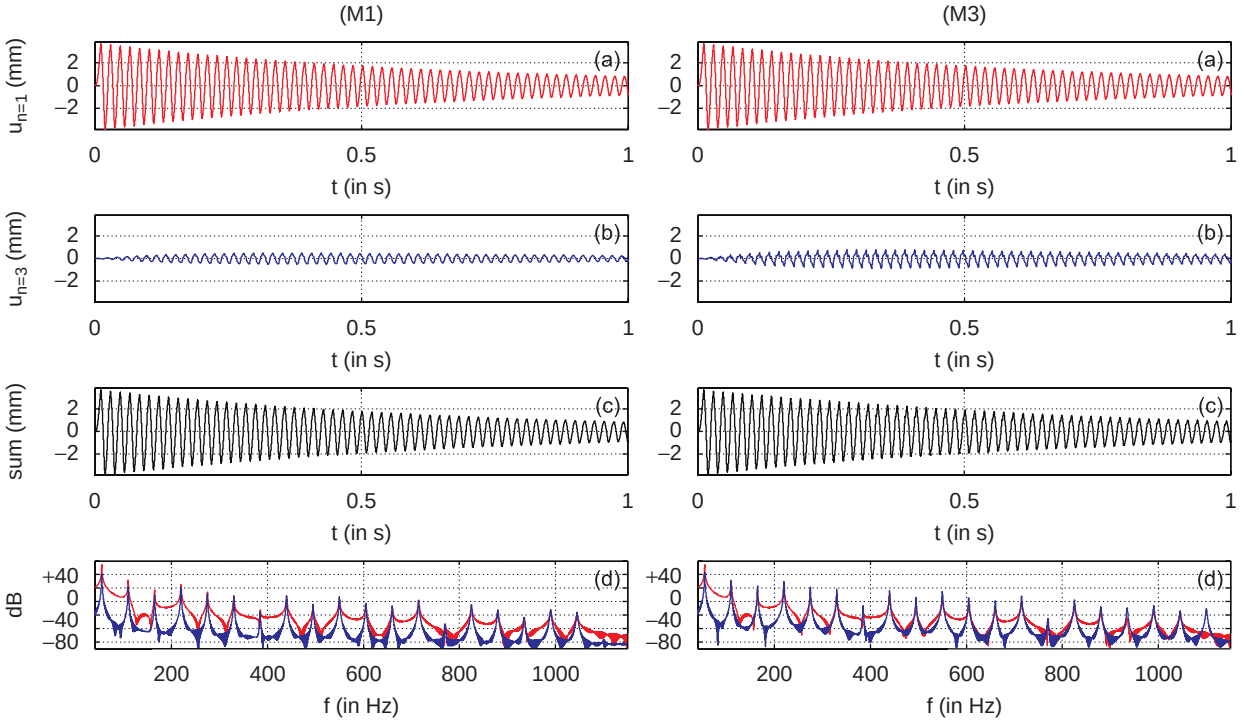

Fig. 24. Idem Fig. 23 with $F^2_{\max} = 20\,\mathrm{N}$.

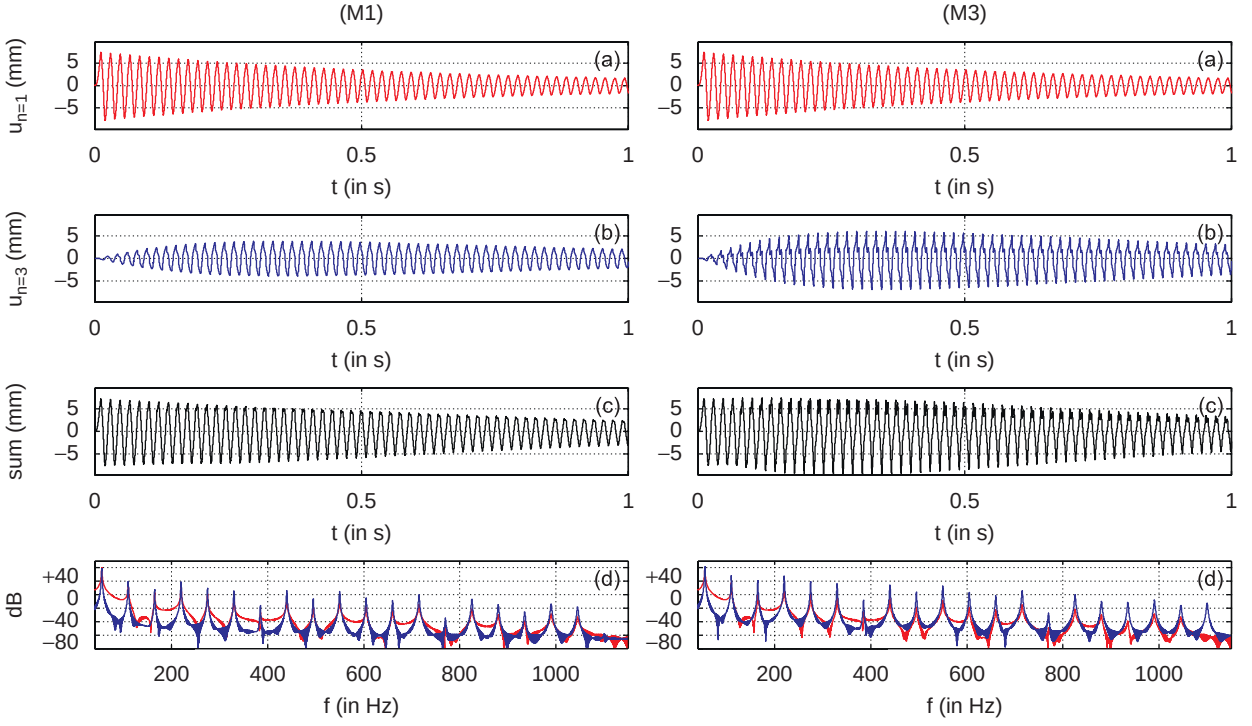

Fig. 25. Idem Fig. 23 with $F^3_{\max} = 40\,\mathrm{N}$.

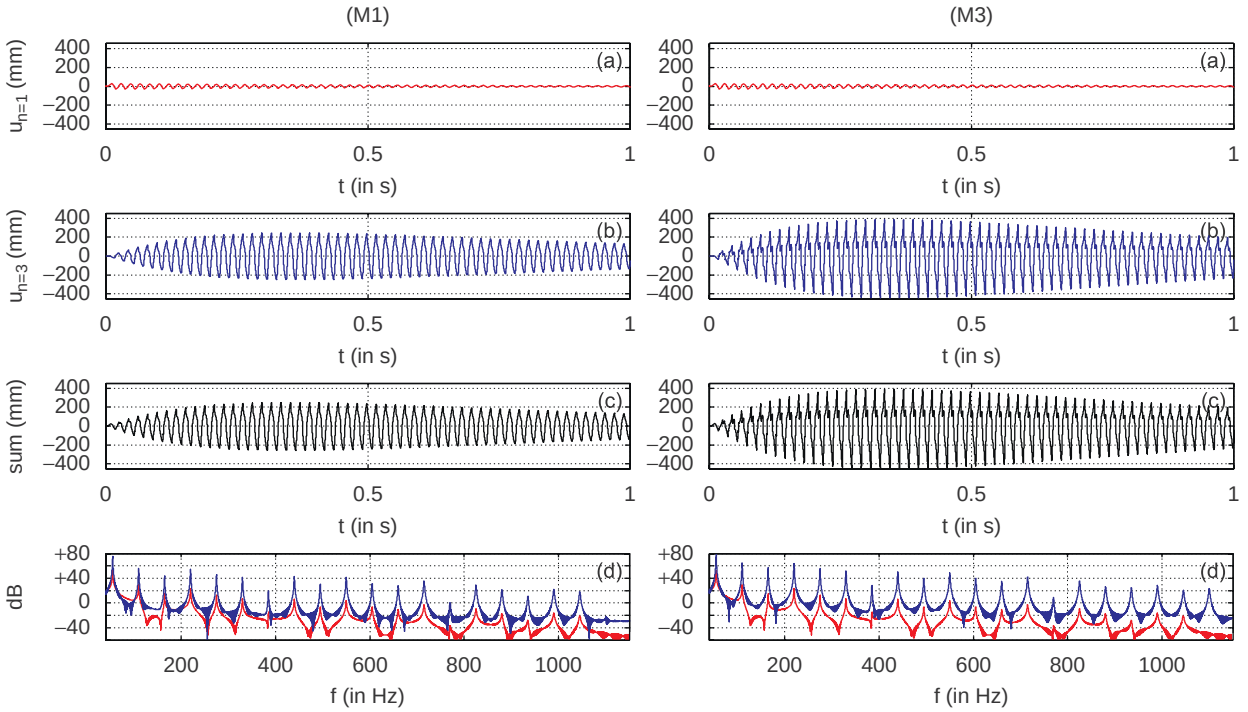

Fig. 26. Idem Fig. 23 with $F^4_{\max} = 160\,\mathrm{N}$.

In practice, such simulations make the estimation of the "operating range" accessible. But, a more rigorous way would consist of deriving the radius of convergence of the series and a bound of the error due to the truncature of the series. Such results can be found for ordinary differential equations with a quadratic nonlinearity [27] but must be generalized to nonlinear partial differential equations.

Estimations of the fundamental frequency [33] make some time-variations appear when the nonlinear contributions are significant. But more discernible is the transfer of energy from the low frequencies to the higher modes through the nonlinear contributions: in Fig. 25, the linear and the nonlinear contributions have similar magnitudes for the first modes (spectrum), while the nonlinear part has more energy than the linear one in the medium and high-frequency range. This is clearly perceptible in the synthesized sounds which are more brilliant at the beginning (before becoming significantly damped). All the more, the transfer of energy is responsible for transients because of its progressive activation (see Figs. 24 and 25 for $0 \leqslant t \leqslant 0.2\,\mathrm{s}$).

Thus, on a specific given "operating range", Volterra series can be an interesting alternative to methods such as nonlinear modes which are limited to particular excitations, or finite difference methods which require the solving of the model overall the domain Ω. With no space discretization, Volterra series can give interesting results at reasonable orders.

7.2. *Higher order approximations ($N = 5$)*

Figs. 27 and 28 detail the contributions at order 5 for the model (M1) and complete Figs. 23–26.

These results corroborate the observations given for order $n = 3$: the contribution at order 5 is negligible for $F^1_{\max}$ ($\max_t|u_5| \approx 9.6 \times 10^{-5}\,\mathrm{mm}$), lower than that of order 3 for $F^2_{\max}$ ($\max_t|u_5| \approx 0.01\,\mathrm{mm}$), similar to that of order 3 for $F^3_{\max}$ ($\max_t|u_5| \approx 3.1\,\mathrm{mm}$), and greater than that of order 3 for $F^4_{\max}$ ($\max_t|u_5| \approx 3226\,\mathrm{mm}$).

Figs. 27 and 28 show that the nonlinear contribution at order 5 requires higher excitation force to appear that at order 3. The transfer of energy from low to high frequencies is more important. In the time domain, this contribution increases more slowly, thus enhancing the "brillance" effect at the beginning of the sound.

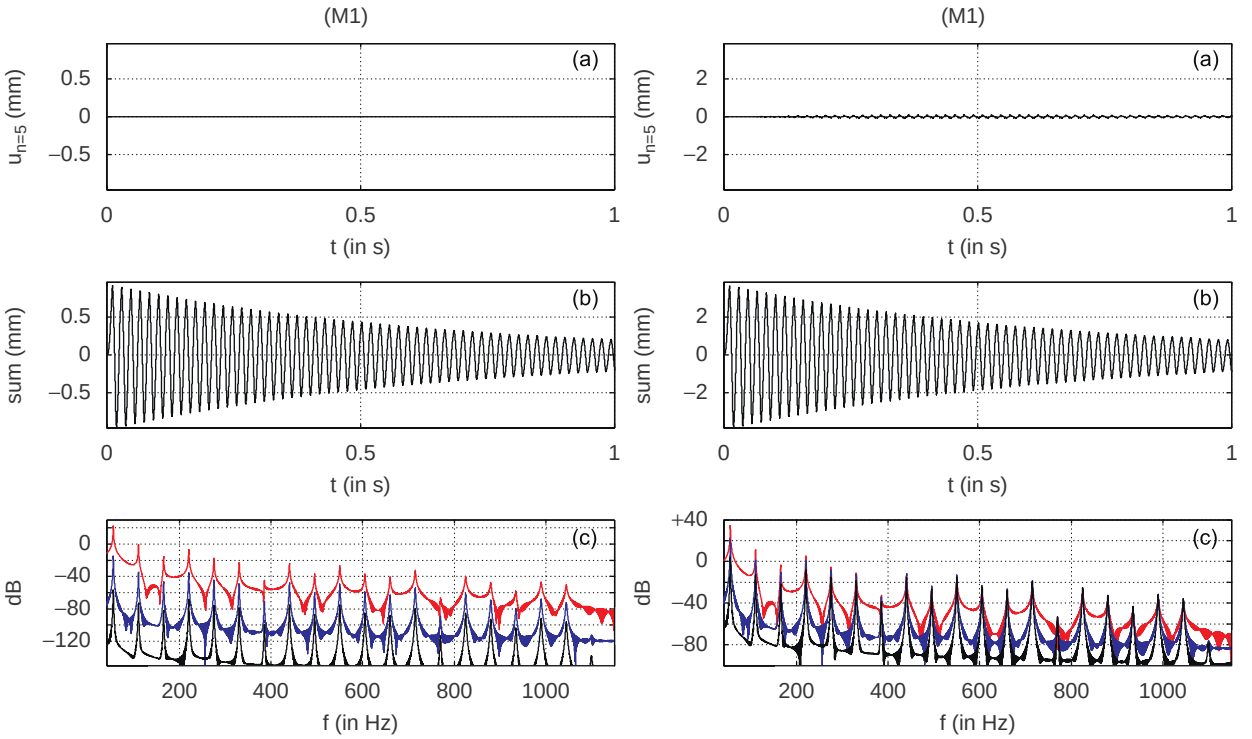

Fig. 27. Simulation of (M1) for $F^1_{\max} = 5\,\mathrm{N}$ and $F^2_{\max} = 20\,\mathrm{N}$. From top to bottom: (a) output of order 5 alone, (b) sum of the contributions up to order 5, and (c) magnitude of the spectrum (order 1, 3, and 5).

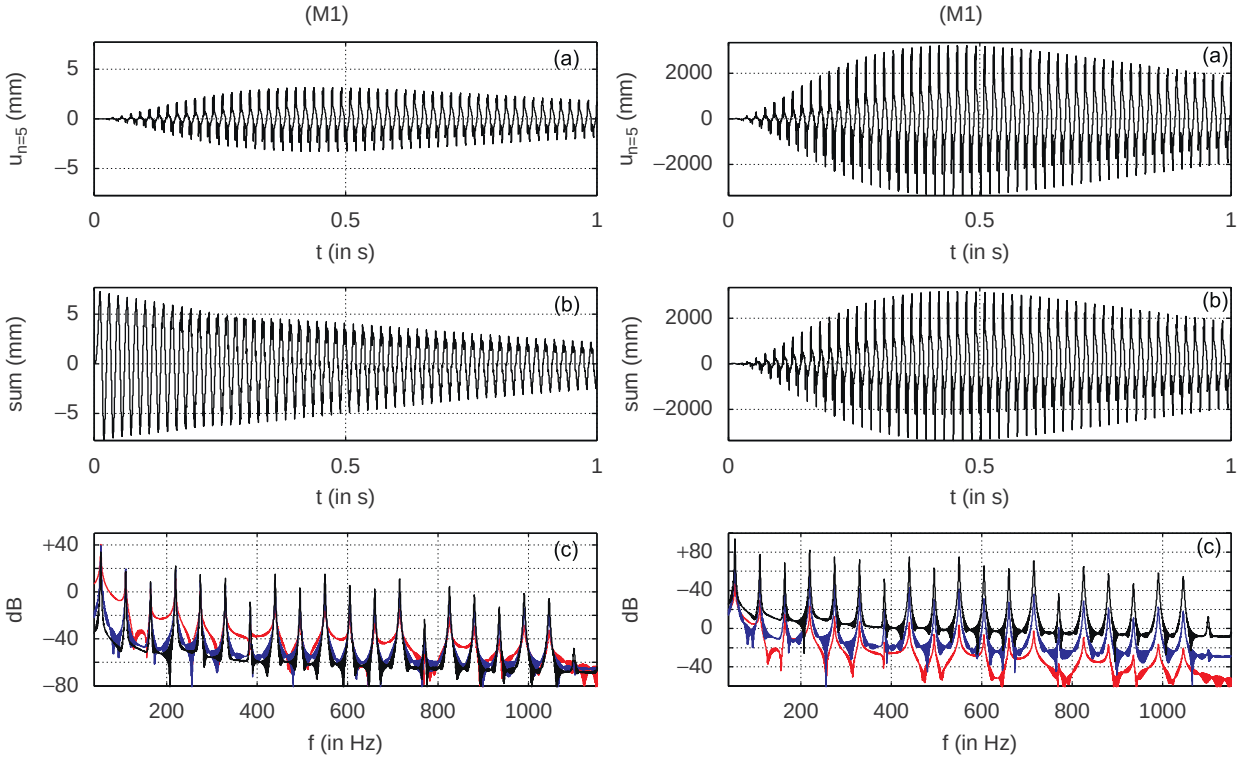

Fig. 28. Idem Fig. 27 for $F^3_{\max} = 40\,\mathrm{N}$ and $F^4_{\max} = 160\,\mathrm{N}$.

8. Conclusion and perspectives

This work has presented an application of Volterra series to simulate nonlinear vibrations of a string. The method proves to be relevant for the (possibly real-time) sound synthesis of some string instruments for which excitations can be quite large. It has been illustrated with three models with one or several located excitations, and global or local nonlinearities. Systematic identifications have allowed the building of structures which give rise to original physical interpretations, and from which efficient algorithms have been deduced. Indeed, these involve only elementary floating point operations (sums and products without infinite loops), the number of which can be precisely estimated.

Nevertheless, the convergence of the series and the estimation of a bound of the error due to truncation are still difficult to tackle. Some future work could focus on this point. Moreover, three-dimensional-string models which take into account coupled waves can be necessary for the naturalness of the sound synthesis. Hence, the study of more accurate models of strings and the analysis of the perception of nonlinear effects by the listener will be part of following works. More generally, using Volterra series could be applied to other physical models (bi- or tri-dimensional), and some other generalizations could be carried out, e.g. extensions to the finite elements method.

Acknowledgements

The authors thank the "Agence Nationale de la Recherche" for supporting this research through the "projet blanc ANR-GIP CONSONNES".

Appendix A

A.1. Green function for the linearized problem: (M1) with $\varepsilon = 0$

Eq. (22) can be written

$$\forall (x, s_{1:n}) \in \Omega \times (\mathbb{C}_0^+)^n, \quad \frac{\partial \mathbf{X}_n^{(x)}(s_{1:n})}{\partial x} = \mathbf{A}(\widehat{s_{1:n}})\mathbf{X}_n^{(x)}(s_{1:n}) + \mathbf{B}(\widehat{s_{1:n}})E_n^{(x)}(s_{1:n}), \tag{98}$$

where

$$\mathbf{X}_n^{(x)}(s_{1:n}) = \begin{bmatrix} H_n^{(x)}(s_{1:n}) \\ \dfrac{\partial H_n^{(x)}(s_{1:n})}{\partial x} \end{bmatrix}, \quad \forall s \in \mathbb{C}_0^+, \quad \mathbf{A}(s) = \begin{bmatrix} 0 & 1 \\ [\Gamma(s)]^2 & 0 \end{bmatrix}, \quad \mathbf{B}(s) = \begin{bmatrix} 0 \\ \dfrac{-1}{1+\beta s} \end{bmatrix},$$

the general solution of which is given by

$$\mathbf{X}_n^{(x)}(s_{1:n}) = \int_0^x \mathrm{e}^{(\xi - x)\mathbf{A}(\widehat{s_{1:n}})}\mathbf{B}(\widehat{s_{1:n}})E_n^{(\xi)}(s_{1:n})\mathrm{d}\xi + \mathrm{e}^{x\mathbf{A}(\widehat{s_{1:n}})}\mathbf{X}_n^{(0)}(s_{1:n}), \tag{99}$$

where

$$\mathrm{e}^{x\mathbf{A}(s)} = \begin{bmatrix} \mathbf{E}_{11}(x,s) & \mathbf{E}_{12}(x,s) \\ \mathbf{E}_{21}(x,s) & \mathbf{E}_{22}(x,s) \end{bmatrix} = \begin{bmatrix} \cosh(x\Gamma(s)) & \sinh(x\Gamma(s))/\Gamma(s) \\ \sinh(x\Gamma(s))\Gamma(s) & \cosh(x\Gamma(s)) \end{bmatrix}.$$

From the boundary conditions Eq. (26), $[1,0]\mathbf{X}_n^{(x)}(s_{1:n}) = 0$ for $x \in \{0;1\}$ which implies, from Eq. (99), that

$$\forall (s_{1:n}) \in (\mathbb{C}_0^+)^n, \quad \frac{\partial H_n^{(0)}(s_{1:n})}{\partial x} = \int_0^1 F(\xi, \widehat{s_{1:n}})E_n^{(\xi)}(s_{1:n})\,\mathrm{d}\xi,$$

with $F(x,s)=\mathbf{E}_{12}(x-1,s)/(1+\beta s)\mathbf{E}_{12}(1,s)$. Hence, denoting $1_{\mathbb{I}}(x)=1$ if $x\in\mathbb{I}$ and $1_{\mathbb{I}}(x)=0$ if $x\notin\mathbb{I}$, Eq. (27) is satisfied with, for all $(x,\xi,s)\in\Omega\times\Omega\times\mathbb{C}_0^+$,

$$G(x,\xi,s)=-1_{[0,x]}(\xi)\frac{\mathbf{E}_{12}(\xi-x,s)}{1+\beta s}+1_{[0,1]}(\xi)\mathbf{E}_{12}(x,s)F(\xi,s), \tag{100}$$

which proves to be also defined by Eq. (28).

A.2. Model (M1): projection of the Volterra kernels on the modal basis

Projecting Eq. (22) on the spatial modes e_k yields:

$$\left\langle [\Gamma(\widehat{s_{1:n}})]^2 H_n^{(x)}(s_{1:n})-\frac{\partial^2 H_n^{(x)}(s_{1:n})}{\partial x^2},e_k\right\rangle=\left\langle \frac{E_n^{(x)}(s_{1:n})}{1+\beta\widehat{s_{1:n}}},e_k\right\rangle, \tag{101}$$

where $E_n^{(x)}$ is defined in Eqs. (23) and (24). Expanding the first member of Eq. (101) and using the linearity of the scalar product yield

$$\begin{aligned}
&\langle [\Gamma(\widehat{s_{1:n}})]^2 H_n^{(x)}(s_{1:n}),e_k\rangle-\left\langle \frac{\partial^2 H_n^{(x)}(s_{1:n})}{\partial x^2},e_k\right\rangle\\
&\quad=[\Gamma(\widehat{s_{1:n}})]^2\langle H_n^{(x)}(s_{1:n}),e_k\rangle-\left\langle H_n^{(x)}(s_{1:n}),\frac{\partial^2 e_k}{\partial x^2}\right\rangle\\
&\quad=[\Gamma(\widehat{s_{1:n}})]^2 H_n^{[k]}(s_{1:n})+(k\pi)^2\langle H_n^{(x)}(s_{1:n}),e_k\rangle\\
&\quad=([\Gamma(\widehat{s_{1:n}})]^2+(k\pi)^2)H_n^{[k]}(s_{1:n}).
\end{aligned} \tag{102}$$

Now, the second member of Eq. (101) is $[1+\beta\widehat{s_{1:n}}]^{-1}\langle E_n^{(x)}(s_{1:n}),e_k\rangle$ where $E_n^{[k]}(s_{1:n})=\langle E_n^{(x)}(s_{1:n}),e_k\rangle$ is given by

$$E_1^{[k]}(s_1)=\langle\phi,e_k\rangle\quad\text{if } n=1, \tag{103}$$

$$E_n^{[k]}(s_{1:n})=\int_0^1 E_n^{(x)}(s_{1:n})e_k(x)\,\mathrm{d}x \tag{104}$$

$$\begin{aligned}
&=\varepsilon\int_0^1\left(\sum_{\substack{p,q,r\geqslant 1\\ p+q+r=n}}\int_0^1\left[\frac{\partial H_p^{(\xi)}(s_{1:p})}{\partial x}\frac{\partial H_q^{(\xi)}(s_{p+1:p+q})}{\partial x}\right]\mathrm{d}\xi\,\frac{\partial^2 H_r^{(x)}(s_{p+q+1:n})}{\partial x^2}e_k(x)\right)\mathrm{d}x\\
&=-\varepsilon\int_0^1\left(\sum_{\substack{p,q,r\geqslant 1\\ p+q+r=n}}\int_0^1\left[\sum_{(\ell_1,\ell_2)\in(\mathbb{N}^*)^2}2\ell_1\ell_2\pi^2\cos(\ell_1\pi\xi)\cos(\ell_2\pi\xi)H_p^{[\ell_1]}(s_{1:p})H_q^{[\ell_2]}(s_{p+1:p+q})\right]\mathrm{d}\xi\right.\\
&\quad\left.\times\left[\sum_{m\in\mathbb{N}^*}2m^2\pi^2 H_r^{[m]}(s_{p+q+1:n})\sin(m\pi x)\sin(k\pi x)\right]\right)\mathrm{d}x
\end{aligned}$$

$$=-\varepsilon k^2\pi^4\sum_{\substack{p,q,r\geqslant 1\\ p+q+r=n}}\sum_{\ell\in\mathbb{N}^*}[\ell^2 H_p^{[\ell]}(s_{1:p})H_q^{[\ell]}(s_{p+1:p+q})]H_r^{[k]}(s_{p+q+1:n})\quad\text{if } n\geqslant 2. \tag{105}$$

Finally, Eqs. (101)–(105) lead to Eqs. (31)–(33) with the definition Eq. (34).

A.3. Proof of Theorem 1

From Remark 5, the kernels $H_n^{(x)}$ with even orders n are null so that Eq. (43) is naturally satisfied from Eq. (41) in Definition 1.

For odd orders, the proof is performed by induction, as follows.

For $n=1$, Eq. (44) is straightforwardly deduced by identification on Eq. (35).

For $n\geqslant 3$, assume that Eqs. (43)–(45) are satisfied for all orders strictly lower than n. Then, from Eq. (24) and under the standard hypotheses of the Lebesgue's dominated convergence theorem (see e.g. Ref. [28]) and the Leibniz integral rule (see e.g. Ref. [25, (3.3.7)]),

$$\begin{aligned} E_n^{(x)}(s_{1,n}) &= \varepsilon \sum_{\substack{p,q,r\geqslant 1\\ p+q+r=n}} \int_0^1 \left(\left[\sum_{\mathfrak{b}\in\mathbb{A}_p} H_{\mathfrak{b}}(s_{1:p}) \frac{\partial e_{\mathfrak{f}(\mathfrak{b})}}{\partial x}(x) \right] \left[\sum_{\mathfrak{c}\in\mathbb{A}_q} H_{\mathfrak{c}}(s_{p+1:p+q}) \frac{\partial e_{\mathfrak{f}(\mathfrak{c})}}{\partial x}(x) \right] \right) \mathrm{d}x \\ &\quad \times \left[\sum_{\mathfrak{d}\in\mathbb{A}_n} H_{\mathfrak{d}}(s_{p+q+1:n}) \frac{\partial^2 e_{\mathfrak{f}(\mathfrak{d})}}{\partial x^2}(x) \right] \\ &= \varepsilon \sum_{\substack{p,q,r\geqslant 1\\ p+q+r=n}} \sum_{(\mathfrak{b},\mathfrak{c},\mathfrak{d})\in\mathbb{A}_p\times\mathbb{A}_q\times\mathbb{A}_r} H_{\mathfrak{b}}(s_{1:p}) H_{\mathfrak{c}}(s_{p+1:p+q}) H_{\mathfrak{d}}(s_{p+q+1:n}) \mathscr{K}_{\mathfrak{b},\mathfrak{c},\mathfrak{d}}(x), \end{aligned} \tag{106}$$

where

$$\begin{aligned} \mathscr{K}_{\mathfrak{b},\mathfrak{c},\mathfrak{d}}(x) &= \left(\int_0^1 \frac{\partial e_{\mathfrak{f}(\mathfrak{b})}}{\partial x}(x). \frac{\partial e_{\mathfrak{f}(\mathfrak{b})}}{\partial x}(x)\,\mathrm{d}x \right) \frac{\partial^2 e_{\mathfrak{f}(\mathfrak{d})}}{\partial x^2}(x) \\ &= -(\pi^2 \mathfrak{f}(\mathfrak{b})\mathfrak{f}(\mathfrak{d}))^2 (\delta_{\mathfrak{f}(\mathfrak{b}),\mathfrak{f}(\mathfrak{c})}) e_{\mathfrak{f}(\mathfrak{d})}(x). \end{aligned} \tag{107}$$

Now, from definitions Eqs. (41) and (42), it follows that

$$\sum_{\substack{p,q,r\geqslant 1\\ p+q+r=n}} \sum_{(\mathfrak{b},\mathfrak{c},\mathfrak{d})\in\mathbb{A}_p\times\mathbb{A}_q\times\mathbb{A}_r} \equiv \sum_{\mathfrak{a}\in\mathbb{A}_n} \tag{108}$$

with $\mathfrak{b}=\mathfrak{a}_1$, $\mathfrak{c}=\mathfrak{a}_2$, $\mathfrak{d}=\mathfrak{a}_3$, $p=\mathfrak{n}(\mathfrak{a}_1)$, $q=\mathfrak{n}(\mathfrak{a}_2)$, $r=\mathfrak{n}(\mathfrak{a}_3)$.

Finally, from Eqs. (31) and (106)–(108), Eq. (43) is satisfied considering the definition Eq. (45) for $H_{\mathfrak{a}}$.

This concludes the proof.

A.4. State-space representation and digital implementation

Consider a mode e_k with $k\in\mathbb{N}^*$ and the associated transfer function $Q^{[k]}(s)$ defined by Eq. (34) with input f and output y. It corresponds to a so-called second-order AR-filter, which admits the following state-space representation:

$$\frac{\mathrm{d}\mathbf{X}}{\mathrm{d}t}(t) = \mathbf{A}\mathbf{X}(t) + \mathbf{B}f(t) \tag{109}$$

$$y(t) = \mathbf{C}\mathbf{X}(t), \tag{110}$$

with

$$\mathbf{X} = \begin{bmatrix} x \\ \dfrac{\mathrm{d}x}{\mathrm{d}t} \end{bmatrix} \quad \mathbf{A} = \begin{bmatrix} 0 & 1 \\ -k^2\pi^2 & -(\alpha+\beta k^2\pi^2) \end{bmatrix}, \quad \mathbf{B} = \begin{bmatrix} 0 \\ 1 \end{bmatrix} \quad \text{and} \quad \mathbf{C} = [1,0]$$

(it can be checked that the transfer function of this system yields $C(s\mathbf{I}_2-\mathbf{A})^{-1}\mathbf{B} = Q^{[k]}(s)$). The solution $\mathbf{X}$ is given by

$$\mathbf{X}(t) = \int_0^t \mathrm{e}^{A(t-\tau)}\mathbf{B}f(\tau)\,\mathrm{d}\tau + \mathrm{e}^{\mathbf{A}t}\mathbf{X}(0),$$

so that, for all $i\in\mathbb{N}$ and $t_i = iT$,

$$\mathbf{X}(t_{i+1}) = \mathrm{e}^{\mathbf{A}T}\mathbf{X}(t_i) + \int_0^T \mathrm{e}^{\mathbf{A}(T-\tau)}\mathbf{B}f(t_i+\tau)\,\mathrm{d}\tau. \tag{111}$$

Note that for a free regime, i.e. when $f(t)=0$, Eq. (111) gives an exact resolution in the discrete-time domain: eigenfrequencies and dampings are exactly preserved. Here, to obtain a numerical simulation, we choose to approximate the input f by a piecewise-linear model $\hat{f}(t)\approx f(t_i)+[(t-t_i)/T][f(t_{i+1})-f(t_i)]$ so that Eq. (111) becomes

$$\mathbf{X}(t_{i+1})=\mathrm{e}^{\mathbf{A}T}\mathbf{X}(t_i)+\mathbf{B}_1 f(t_i)+\mathbf{B}_0 f(t_{i+1}), \tag{112}$$

with $\mathbf{B}_1=T^{-1}\mathbf{A}^{-2}[\mathbf{I}_2-(\mathbf{I}_2-T\mathbf{A})\mathrm{e}^{\mathbf{A}T}]\mathbf{B}$ and $\mathbf{B}_0=T^{-1}\mathbf{A}^{-2}[-(\mathbf{I}_2+T\mathbf{A})+\mathrm{e}^{\mathbf{A}T}]\mathbf{B}$. Now, from Eq. (112),

$$\begin{aligned} y(t_{i+2})=\mathbf{C}(&\mathrm{e}^{\mathbf{A}T}(\mathrm{e}^{\mathbf{A}T}\mathbf{X}(t_i)+\mathbf{B}_1 f(t_i)+\mathbf{B}_0 f(t_{i+1}))\\ &+\mathbf{B}_1 f(t_{i+1})+\mathbf{B}_0 f(t_{i+2})), \end{aligned} \tag{113}$$

$$\begin{bmatrix} y(t_{i+1})\\ y(t_i)\end{bmatrix}=\underbrace{\begin{bmatrix}\mathbf{C}\mathrm{e}^{\mathbf{A}T}\\ \mathbf{C}\end{bmatrix}}_{\boldsymbol{\kappa}\ \text{(invertible)}}\mathbf{X}(t_i)+\begin{bmatrix}\mathbf{C}\mathbf{B}_1\\ 0\end{bmatrix}f(t_i)+\begin{bmatrix}\mathbf{C}\mathbf{B}_0\\ 0\end{bmatrix}f(t_{i+1}). \tag{114}$$

Then, isolating $\mathbf{X}(t_i)$ in Eq. (114) and substituting this solution Eq. (113) yields the recursive (scalar) equation

$$y(t_{i+2})=a_1 y(t_{i+1})+a_2 y(t_i)+b_0 f(t_{i+2})+b_1 f(t_{i+1})+b_2 f(t_i), \tag{115}$$

with computable coefficients (a_1,a_2,b_0,b_1,b_2). *This equation is used for the simulation: it requires* $N_q^+=4$ *sums and* $N_q^\times=5$ *products, at each step.*

References

[1] S. Bilbao, J.O. Smith III, Energy-conserving difference schemes for nonlinear strings, *Acta Acustica United with Acustica*, 2005, pp. 299–311.

[2] C. Touzé, Analyse et Modélisation de Signaux Acoustiques et Vibratoires Chaotiques, Application aux Instruments de Percussion Non-linéaires. PhD Thesis, ENST, 2000.

[3] S.W. Shaw, C. Pierre, Normal modes of vibration for non-linear continuous systems, *Journal of Sound and Vibration* 169 (1994) 319–347.

[4] M.S. Nakhla, J. Vlach, A piecewise harmonic balance technique for determination of periodic response of nonlinear systems, *IEEE Transactions on Circuits and Systems* 23 (1976) 85–91.

[5] L. Menguy, J. Gilbert, Weakly non-linear gas oscillation in air-filled tubes: solutions and experiment, *Acta Acustica* 86 (2000) 798–810.

[6] Th. Hélie, M. Hasler, Volterra series for solving weakly non-linear partial differential equations: application to a dissipative burger's equation, *International Journal of Control* 77 (12) (2004) 1071–1082.

[7] Th. Hélie, Résolution d'une équation des ondes faiblement non-linéaire par les séries de Volterra et décomposition modale. In *Congrès Français d'Acoustique*, Tours, 2006.

[8] J. Le Rond d'Alembert, Recherches sur la courbe que forme une corde tendue mise en vibration, *Mémoires de l'académie des Sciences de Berlin*, 1747, pp. 214–219.

[9] L. Euler, Sur la vibration des cordes, *Mémoires de l'académie des Sciences de Berlin*, 1750, pp. 69–85.

[10] C. Truesdell, Outline of the history of flexible or elastic bodies to 1788, *Journal of the Acoustical Society of America* 32 (12) (1960) 1647–1656.

[11] G. Kirchhoff, *Vorlesungen über Mathematische Physik: Mechanik*, Teubner, Leipzig, 1877.

[12] G.F. Carrier, On the non-linear vibration problem of the elastic string, *Quarterly of Applied Mathematics* 3 (1945) 157–165.

[13] G.V. Anand, Large-amplitude damped free vibration of a stretched string, *Journal of the Acoustical Society of America* 45 (5) (1969) 1089–1096.

[14] R. Narasimha, Non-linear vibration of an elastic string, *Journal of Sound and Vibration* 8 (1968) 134–146.

[15] A. Watzky, Non-linear three-dimensional large-amplitude damped free vibration of a stiff elastic stretched string, *Journal of Sound and Vibration* 153 (1992) 125–142.

[16] C. Valette, Ch. Cuesta, *Mécanique de la corde vibrante*, Hermès, 1993.

[17] A. Chaigne, V. Doutaut, Numerical simulations of xylophones. I. Time-domain modeling of the vibrating bars, *Journal of the Acoustical Society of America* 101 (1997) 539–557.

[18] GoC. Gorain, S.K. Bose, Uniform stability of damped nonlinear vibrations of an elastic string, *Proceedings of the Indian Academy of Sciences* (*Mathematical Sciences*) Vol. 113 (4) (November 2003) pp. 443–449.

[19] M.F. Ashby, *Materials Selection in Mechanical Design*, Butterworth-Heinemann, 2004.

[20] Source for materials information, ⟨http://www.matweb.com⟩.

[21] S.P. Boyd, Volterra Series: Engineering Fundamentals, PhD Thesis, Harvard University, 1985.

[22] M. Hasler, *Systèmes non linéaires*, EPFL, Lausanne, 1999.
[23] W.J. Rugh, Nonlinear system theory, Web Version, 2002.
[24] F. Lamnabhi-Lagarrigue, *Analyse des Systèmes Non Linéaires*, Hermès, 1994.
[25] M. Abramowitz, I.A. Stegun, *Handbook of Mathematical Functions*, Dover, New York, 1970.
[26] S. Boyd, L.O. Chua, Fading memory and the problem of approximating nonlinear operators with Volterra series, *IEEE Transactions of Circuits and Systems* 32 (1985) 1150–1161.
[27] Th. Hélie, B. Laroche, On the convergence of Volterra series of finite dimensional quadratic MIMO systems, *International Journal of Control*, Special issue in Honor of Michell Fliess 60th-birthday, 81 (3) (2008).
[28] S. Browder, *Mathematical Analysis: An Introduction*, Springer, New York, 1996.
[29] H. Brézis, *Analyse Fonctionnelle*, *Théorie et Applications*. Dunod, 1999.
[30] Th. Hélie, D. Matignon, Damping models for the sound synthesis of bar-like instruments, *Seventh International Conference on Systemics*, *Cybernetics and Informatics*, *Orlando*, *Florida*, July 2001, pp. 541–546.
[31] D. Roze, Simulation d'une Corde avec fortes Déformations par les Séries de Volterra. Master's Thesis, Université Pierre et Marie Curie, Paris 6, 2006.
[32] L.R. Rabiner, C.M. Rader (Eds.), *Digital Signal Processing*, IEEE Press, Inc., New York, 1972.
[33] A. de Cheveigné, H. Kawahara, Yin, a fundamental frequency estimator for speech and music, *Journal of the Acoustical Society of America* 111 (2002) 1917–1930.